NASA Technical Memorandum 86402

Determination of Corrections to Flow Direction Sensor Measurements Over an Angle-of-Attack Range From 0° to 85°

Thomas M. Moul

DECEMBER 1985

NASA

NASA Technical Memorandum 86402

Determination of Corrections to Flow Direction Sensor Measurements Over an Angle-of-Attack Range From 0° to 85°

Thomas M. Moul
Langley Research Center
Hampton, Virginia

NASA
National Aeronautics
and Space Administration
Scientific and Technical Information Branch
1985

Summary

An investigation has been conducted into the nature of corrections for flow direction measurements obtained with wingtip-mounted sensors. Corrections have been determined for the angles of attack and sideslip measured by sensors mounted in front of each wingtip of a rectangular-wing general aviation airplane. These flow corrections have been obtained from both wind-tunnel and flight tests over an angle-of-attack range from 0° to 85°. Both the angle-of-attack and angle-of-sideslip flow corrections were found to be substantial. The corrections were a function of the angle of attack and angle of sideslip. The effects of wing configuration changes and spinning rotation on the angle-of-attack flow correction were found to be small. The angle-of-attack flow correction determined from the static wind-tunnel tests agreed reasonably well with the correction determined from flight tests.

Introduction

In quantitative flight test investigations it is often desirable to reduce the flight data to a form that can be compared directly with wind-tunnel data or theoretical predictions. An essential flight quantity for this comparison is the true angle of attack of the airplane. Typically, the angle of attack during flight tests is measured with a self-aligning vane or flow direction sensor (ref. 1). For single-engine general aviation airplanes, the sensors are often mounted on booms ahead of the wing near each wingtip and measure the local flow direction. To determine the true angle of attack of the airplane, corrections must be applied to this measured local flow direction (called the measured angle of attack herein) to account for the change in the flow direction at the sensor locations because of the presence of the airplane.

For airplanes in the normal, unstalled flight regime, this flow correction may be easily determined both experimentally and theoretically (ref. 2). Experimentally, when an airplane is in steady, straight and level flight, the true angle of attack is given either by the pitch attitude measurement or by the inverse sine of the longitudinal acceleration measurement (refs. 3 and 4). Theoretically, the flow correction in front of the wing may be determined by using lifting line theory (refs. 5 and 6).

However, at angles of attack above the stall, most of these methods are no longer usable. The flight test technique cannot be used because the airplane can no longer achieve steady level flight at angles of attack above the stall. Also, the lifting line theory is no longer valid because of the separated flow over the wing. In fact, the nature of the flow correction at these large angles of attack is not well-known.

One field of study in which the knowledge of this flow correction at large angles of attack is needed is in spin flight testing. At the large angles of attack encountered during spin flight tests, the flow correction is substantial and, therefore, must be applied to the flight data to enable correlation with data from other sources (ref. 7). Also, any theoretical methods used in predicting or analyzing spin characteristics would require the true angle of attack to be known. Thus, an understanding of the flow correction at large angles of attack is important in the study of spinning flight.

Preliminary investigations into the nature of the flow correction at large angles of attack have shown that the correction can be substantial (refs. 8 and 9). However, these reports looked only briefly at the flow correction encountered on one general aviation configuration. Thus, it was deemed necessary to undertake a more extensive study of flow correction and to obtain flow correction data for a different general aviation configuration.

This paper presents the results of a study to determine the flow corrections to be applied to the measurement of the angles of attack and sideslip over a large angle-of-attack range. This paper is a shortened version of a thesis (ref. 10) that was submitted in partial fulfillment of the requirements for the Degree of Master of Science at George Washington University, Washington, D.C., August 1983. The present work includes the determination of the flow correction from both wind-tunnel and flight tests of a general aviation research airplane.

A 1/6-scale model of the general aviation research airplane was tested in the Langley 12-Foot Low-Speed Tunnel. The model was tested over a large angle-of-attack range, and the effects on the flow correction due to changes in flow parameters and configuration changes were determined. The same model was also tested on the rotary-balance apparatus located in the Langley Spin Tunnel. The model was tested up to an angle of attack of 90° at different rates of rotation.

The general aviation research airplane was flown in steady, straight and level flight to obtain a low-angle-of-attack flow correction. The same airplane was used to gather data during extensive spin flight testing. Three different analytical methods were applied to the data to determine the flow correction during spinning flight.

Symbols

Quantities were measured with respect to the stability axes, ground axes, and body axes. The body

system of axes with definitions and sign convention of some of the measurements are shown in figure 1. Values are given in the International System of Units (SI) with equivalent values in U.S. Customary Units. Conversion factors are found in reference 11. Measurements and calculations were made in U.S. Customary Units.

$\mathbf{A}$	resultant-acceleration vector, g units
A_c	centrifugal acceleration, m/sec^2 (ft/sec^2)
$\mathbf{A}_X, \mathbf{A}_Z$	linear-acceleration vectors along X_g and Z_g ground axes, respectively, g units
a_w	acceleration along velocity vector, g units
a_x, a_y, a_z	linear accelerations along X_b, Y_b, and Z_b body axes, respectively, g units
b	wing span, m (ft)
C	constant, $(1 + a_y \sin\beta)/\cos\beta$
C_D	drag coefficient, Drag/$q_\infty S$
C_L	lift coefficient, Lift/$q_\infty S$
C_R	resultant-force coefficient, $(C_D^2 + C_L^2)^{1/2}$
C_m	pitching-moment coefficient, positive nose up, Pitching moment/$q_\infty S\bar{c}$
$\bar{c}$	wing mean aerodynamic chord, m (ft)
F_g	gravity force, N (lb)
F_w	force along velocity vector, N (lb)
g	acceleration due to gravity (where $1g = 9.81$ m/sec^2 (32.17 ft/sec^2))
h	altitude, m (ft)
$\dot{h}$	altitude rate, m/sec (ft/sec)
I,J,K	unit vectors along X_g, Y_g, and Z_g ground axes, respectively
i, j, k	unit vectors along X_b, Y_b, and Z_b body axes, respectively
i, j, k	direction components of $\mathbf{X}'_g$ in body axes
K_α	misalignment of boom in angle-of-attack direction at $0g$, deg
K_β	misalignment of boom in angle-of-sideslip direction at $0g$, deg
$\mathbf{L}_{bw}$	transformation matrix from wind axes to body axes
ℓ_J, m_J, n_J	direction cosines in body axis system of J ground axis
ℓ'_j, m'_j, n'_j	direction cosines in ground axis system of j body axis
m	mass, kg (slugs)
p, q, r	angular velocity about X_b, Y_b, and Z_b body axes, respectively, deg/sec
q_∞	free-stream dynamic pressure, Pa (lb/ft^2)
R	Reynolds number, $V_T\bar{c}/\nu$
R_S	radius of spin, m (ft)
S	wing area, m^2 (ft^2)
U, V, W	linear velocities along X_g, Y_g, and Z_g ground axes, respectively, m/sec (ft/sec)
u, v, w	linear velocities along X_b, Y_b, and Z_b body axes, respectively, m/sec (ft/sec)
V_T	total velocity, m/sec (ft/sec)
$\mathbf{V}_T$	total-velocity vector, m/sec (ft/sec)
$V_{T,c}$	local-flow total velocity with boom and flow direction sensor in calibration apparatus, m/sec (ft/sec)
$V_{T,m}$	local-flow total velocity with boom and flow direction sensor mounted on model, m/sec (ft/sec)
X_b, Y_b, Z_b	body axes
X_g, Y_g, Z_g	ground axes
$\mathbf{X}'_g$	vector along X_g ground axis
x, y, z	distance along X_b, Y_b, and Z_b body axes, respectively, from c.g. to flow direction sensors, m (ft)
α	angle of attack, deg
α_a	change in angle of attack caused by mounting boom bending under static air load, deg
α_b	change in angle of attack caused by mounting boom bending under inertial load, deg

α_d	change in angle of attack caused by vehicle rotation, deg
α_m	measured angle of attack, deg
$\bar{\alpha}_m$	average measured angle of attack, $\frac{\alpha_{m,R}+\alpha_{m,L}}{2}$, deg
α_t	true angle of attack, deg
$\bar{\alpha}_t$	average true angle of attack, $\frac{\alpha_{t,R}+\alpha_{t,L}}{2}$, deg
α_u	change in angle of attack caused by upwash from mounting boom, deg
α_v	angle-of-attack vane floating angle (caused by mass unbalance or by warp in vane surface), deg
β	angle of sideslip, deg
β_a	change in sideslip angle caused by mounting boom bending under static air load, deg
β_b	change in sideslip angle caused by mounting boom bending under inertial load, deg
β_d	change in sideslip angle caused by vehicle rotation, deg
β_m	measured angle of sideslip, deg
$\bar{\beta}_m$	average measured angle of sideslip, $\frac{\beta_{m,R}+\beta_{m,L}}{2}$, deg
β_s	change in sideslip angle caused by sidewash from mounting boom, deg
β_t	true angle of sideslip, deg
β_v	sideslip-vane floating angle (caused by warp in vane surface), deg
γ	flight path angle, deg
δ	helix angle of flight path measured from the vertical, deg
δ_a	aileron deflection, deg
ϵ_α	angle-of-attack flow correction, deg
ϵ_α	average angle-of-attack flow correction, $\frac{\epsilon_{\alpha,R}+\epsilon_{\alpha,L}}{2}$, deg
ϵ_β	angle-of-sideslip flow correction, deg
ϵ_β	average angle-of-sideslip flow correction, $\frac{\epsilon_{\beta,L}-\epsilon_{\beta,R}}{2}$, deg
θ	airplane pitch attitude, deg
θ_{st}	model mounting strut angle, deg
μ	angle between flight path and X_b body axis, deg
ν	kinematic viscosity, m^2/sec (ft^2/sec)
σ	angle between resultant-acceleration and resultant-rotation vectors, deg
Ω	angular velocity about spin axis, deg/sec
$\boldsymbol{\Omega}$	angular-velocity vector, deg/sec
$\Omega b/2V_T$	spin coefficient, positive for clockwise spins

Subscripts:

b	body axis system
cg	at center-of-gravity location
L	left
m	measured
R	right
s	at sensor location
w	wind axis system

Abbreviation:

c.g.	center of gravity

Background

The angles of attack and sideslip are often measured in flight by flow direction sensors mounted on booms attached to the airplane. To determine the true angles of attack and sideslip, a number of corrections must be applied to the indicated measurements of the sensors. The correction equations, taken from reference 12, with some modifications, are

$$\alpha_t = \alpha_m - \epsilon_\alpha - \alpha_d - \alpha_a - \alpha_b - \alpha_u - \alpha_v - K_\alpha \quad (1)$$

$$\beta_t = \beta_m - \epsilon_\beta - \beta_d - \beta_a - \beta_b - \beta_s - \beta_v - K_\beta \quad (2)$$

If care is taken in the design, manufacture, and installation of the mounting boom and sensors, many of these terms can be neglected. In this paper the following correction equations will be used:

$$\alpha_t = \alpha_m - \epsilon_\alpha - \alpha_d \quad (3)$$

$$\beta_t = \beta_m - \epsilon_\beta - \beta_d \quad (4)$$

During the static wind-tunnel tests, the model was not rotating and the equations may be simplified to yield

$$\alpha_t = \alpha_m - \epsilon_\alpha \quad (5)$$

$$\beta_t = \beta_m - \epsilon_\beta \quad (6)$$

Test Configurations

Flight Test Airplane

A single-engine, low-wing, general aviation spin research airplane (fig. 2) was used in the flight tests reported herein. A three-view drawing of the airplane is shown in figure 3. Some of the pertinent physical characteristics of the airplane are given in table I.

The test airplane was equipped with a flow direction and velocity sensor (ref. 1) mounted on a boom ahead of each wingtip (fig. 4). Each sensor pivot was located 1.06 m (3.49 ft) or $0.79\bar{c}$ in front of the wing and 4.41 m (14.47 ft) or $0.88b/2$ outboard from the airplane centerline. The sensors measured the angles of attack and sideslip and the true airspeed of the airplane. The angle-of-attack and angle-of-sideslip sensors were calibrated before each flight. The accuracy of the angle-of-sideslip sensor was about $\pm 1/2°$ whereas the accuracy of the angle-of-attack sensor was about $\pm 1°$ (ref. 3).

Modifications to the wing and body were flight tested to evaluate their effect on the spin characteristics of the airplane. One of the wing modifications was found to improve the spin resistance of this class of airplanes (ref. 13). This modification consisted of a glove over the forward part of the airfoil that provided a 3-percent-chord extension and a droop that increased the leading-edge camber and radius (fig. 5). This leading-edge droop modification could be added to the full span of the airplane wing, but it was segmented so that different spanwise lengths could also be tested.

The research airplane was also equipped with hydrogen peroxide rockets mounted on each wingtip (ref. 14). The rockets could be used to stop the airplane from spinning or to increase the spin rate of the airplane.

Wind-Tunnel Model

A 1/6-scale model of the spin research airplane was tested in the Langley 12-Foot Low-Speed Tunnel and in the Langley Spin Tunnel. The model had neither landing gear nor a propeller. The rear fuselage section, including the horizontal and vertical tails, was removed to facilitate mounting the model in the 12-Foot Wind Tunnel. A drawing of the model as tested in the 12-Foot Tunnel is shown in figure 6. In the Spin Tunnel the model was tested with both the horizontal and vertical tails on.

The model was equipped with two flow direction sensors (fig. 7) that were similar to those used on the research airplane. The flow direction sensors were mounted on 6.35-mm-diameter (0.25-in.) cylindrical rods that positioned the sensors in front of each wingtip. The sensor pivot was located 17.7 cm (6.97 in.) or $0.79\bar{c}$ in front of the leading edge of the wing. The pivot was located 73.4 cm (28.9 in.) or $0.88b/2$ outboard from the centerline of the model. This sensor location corresponded to the sensor location on the full-scale research airplane. The sensors measured the local angles of attack and sideslip. The angle-of-attack measurements were repeatable within $\pm 1°$ and the angle-of-sideslip measurements were repeatable within $\pm 2°$.

The model had movable ailerons allowing deflections up to $\pm 25°$. A scaled version of the leading-edge droop modification tested in flight could be applied to the forward portion of the model airfoil. This droop modification was also segmented so that different spanwise lengths could be tested.

Test Techniques and Conditions

Wind-Tunnel Tests

Static tests. The 1/6-scale model of the research airplane was tested in the Langley 12-Foot Low-Speed Tunnel, which has a 3.66 m (12 ft) octagonal test section. Figure 8 shows the model mounted in the wind tunnel. To help understand the basic nature of the flow corrections, aerodynamic forces and moments acting on the model were measured with an internally mounted, six-component, strain-gauge balance. The moment data were nondimensionalized and presented as body axis rolling-, yawing-, and pitching-moment coefficients for a center-of-gravity position of $0.21\bar{c}$. The force data were nondimensionalized and transferred to the stability axis system and presented as lift, drag, and side-force coefficients.

Most of the tests were conducted at a free-stream dynamic pressure of 19.5 kg/m^2 (4 psf), which corresponded to a velocity of 17.7 m/sec (58.0 ft/sec) and a Reynolds number of 0.27×10^6, based on the mean aerodynamic chord of the wing. The model was tested over an angle-of-attack range from 0° to 85° and an angle-of-sideslip range from −20° to 20°. Because the force and moment data were used only to show trends, the data were not corrected for tunnel upwash (about 2° for this test).

The leading-edge droop modification discussed previously was tested in two lengths. The outboard droop extended from $0.57b/2$ to $0.95b/2$ on each wing and the full-span droop extended from the fuselage to $0.95b/2$ on each wing. The effects of aileron deflections, sensor location, and angle of sideslip on the flow corrections were also investigated.

To account for flow irregularities in the tunnel, a calibration was conducted. To accomplish this, the booms and sensors were removed from the model and placed in a calibration apparatus. This apparatus positioned the booms and sensors at the same point in the tunnel as they were when mounted on the model. With the model out of the tunnel and the booms and sensors in this calibration setup, the sensors measured the true or free-stream angles of attack and sideslip as a function of the model mounting strut angle θ_{st} (fig. 9(a)). Calibration runs were made at angles of sideslip from $-20°$ to $20°$ and at angles of attack from $0°$ to $85°$.

After the calibration runs were made, the booms and sensors were mounted on the model and the model tests were conducted. In this configuration the sensors gave the measured angles of attack and sideslip as a function of the mounting strut angle (fig. 9(b)).

Rotary tests. The 1/6-scale model of the research airplane was also tested in the Langley Spin Tunnel using the rotary-balance apparatus (fig. 10 and ref. 15). A six-component strain-gauge balance was used to measure the forces and moments acting on the model while subjected to rotational-flow conditions. The data were nondimensionalized and presented as body axis force and moment coefficients for a center-of-gravity position of $0.21\bar{c}$.

The tests were conducted at an airstream velocity of 7.6 m/sec (25 ft/sec), which corresponded to a Reynolds number of 0.12×10^6, based on the mean aerodynamic chord of the wing. The model was tested over an angle-of-attack range from $8°$ to $90°$. For angles of attack from $30°$ to $90°$ the model rotated such that the spin axis passed through the full-scale airplane c.g. location. For angles of attack from $8°$ to $35°$, the spin axis was set 30.48 cm (12 in.) in front of the c.g. location. At each angle of attack both static and rotary data were obtained. The rates of rotation included values of $\Omega b/2V_T$ of 0.1, 0.2, 0.3, 0.4, 0.5, 0.6, 0.7, 0.8, and 0.9 in both clockwise and counterclockwise directions.

A calibration to account for flow irregularities in the Spin Tunnel was not conducted. It was felt that a flow calibration was not as necessary in the Spin Tunnel as it was in the 12-Foot Tunnel. This was due to the fact that during the rotary tests, data were taken as the flow direction sensors swept around the tunnel, thus helping to average out some of the flow irregularities.

Flight Tests

An analog data system with 20 channels of continuous frequency-modulated data and 28 channels of time-shared pulse amplitude modulated (PAM) data was installed on the research airplane. The measured data were stored on a 9-track magnetic tape at a rate of 20 times per second. The measured parameters included the true airspeed and flow angles ahead of each wingtip, linear accelerations, angular rates, Euler attitudes, control positions and forces, altitude, and altitude rate. Table II shows the measurements used herein to calculate the flow corrections in flight.

Level flight tests. The spin research airplane was flown in steady, straight and level flight at different airspeeds to obtain an airspeed and angle-of-attack calibration. Data were taken at airspeeds ranging from 34.95 m/sec (67.93 knots) to 54.23 m/sec (105.41 knots). The Reynolds number varied from 3.16×10^6 to 4.89×10^6 with an average of 3.91×10^6. At each airspeed the airplane was flown over a ground course in opposite directions and the results of the two runs were averaged. From these tests a low-angle-of-attack flow correction was determined.

Spin flight tests. The research airplane was flight tested as part of the general aviation stall/spin program at the Langley Research Center. The spin flight tests were conducted at the NASA Wallops Flight Facility following the procedures described in reference 16. During the spin research program the airplane was flown with different center-of-gravity locations and with a number of different leading-edge droop modifications. On some of the spin flights the rocket system was fired in a pro-spin direction in order to look for high-angle-of-attack spin modes. These different conditions resulted in the airplane spinning at different angles of attack over a fairly large angle-of-attack range. This angle of attack caused the Reynolds number to vary during the spin tests from 1.95×10^6 to 3.85×10^6 with an average of 2.68×10^6. Three analytical methods and data from 15 steady spins were used to calculate the flow corrections of the spinning airplane.

Reynolds Number Effects

The Reynolds number during the wind-tunnel tests was approximately a factor of 10 lower than the Reynolds numbers during the flight tests. Specifically, the Reynolds number was 0.27×10^6 during the static tests and 0.12×10^6 during the rotary tests, although the Reynolds number averaged 3.91×10^6 during the level flight tests and 2.68×10^6 during the spin flight tests. This Reynolds number difference can make it difficult to compare wind-tunnel results exactly with flight results. A model of a different general aviation configuration was tested in another NASA wind tunnel in which the test Reynolds

number could be varied over a large range (ref. 17). Figure 11 compares the lift coefficient of that model tested at two Reynolds numbers. The low Reynolds number is close to the value of the Reynolds number during the wind-tunnel tests, and the high Reynolds number is close to the Reynolds number during slow flight. The figure shows the well-known increase in maximum lift coefficient as well as the stall angle of attack with an increase of the Reynolds number (ref. 18).

Although the Reynolds number effect on the wind-tunnel flow correction data may be significant, this effect has not been determined. As a result, the wind-tunnel-determined flow correction should be applied with caution to full-scale flight data and can be used to provide only an approximate estimate of the true angle of attack of the airplane.

Analysis Techniques

Static Wind-Tunnel Tests

Angle-of-attack flow correction. To determine the angle-of-attack flow correction, data from the desired model-installed run as well as data from the appropriate calibration run were used. The angle-of-attack flow correction ϵ_α was the difference between the measured and the true angles of attack at a particular strut angle (fig. 12(a)); that is,

$$\epsilon_\alpha = \alpha_m - \alpha_t \tag{7}$$

To help account for flow-field irregularities and/or asymmetries in the model, the angle-of-attack flow correction measured with the right sensor was averaged with the flow correction from the left sensor. This average angle-of-attack flow correction was then plotted against the average of the measured angles of attack from the left and right sensors.

To look at the effect of sideslip angle on the angle-of-attack flow correction, the flow correction was plotted against the measured angle of attack for three values of sideslip. As the model was sideslipped, the angle-of-attack flow correction increased at one sensor location and decreased at the other. Thus, the average of the angle-of-attack flow correction from the left and right sensors did not change much as the model was sideslipped. Therefore, in order to present the effect of the sideslip angle, the angle-of-attack flow correction from the right sensor was plotted against the measured angle of attack from the right sensor. In this case, data from the right sensor were used because these data were more consistent than the data from the left sensor.

Angle-of-sideslip flow correction. The angle-of-sideslip flow correction was determined in a manner similar to the method used in the calculation of the angle-of-attack flow correction. That is, the angle-of-sideslip flow correction ϵ_β was the difference between the measured and true angles of sideslip at a particular strut angle (fig. 12(b)); that is,

$$\epsilon_\beta = \beta_m - \beta_t \tag{8}$$

The angle-of-sideslip flow correction was also averaged, but in a slightly different manner. As the angle of attack increased, the noses of the sideslip sensors had a tendency to point toward the centerline of the model. This represented a positive sideslip increment for the left sensor and a negative sideslip increment for the right sensor. Thus, if the angle-of-sideslip flow correction from both sensors was simply averaged, the resulting correction would be close to 0. To determine the magnitude of the angle-of-sideslip flow correction, the correction from the right sensor was subtracted from the correction measured by the left sensor and the result was divided in half. That is,

$$\bar{\epsilon}_\beta = \frac{\epsilon_{\beta,L} - \epsilon_{\beta,R}}{2} \tag{9}$$

This averaged magnitude of the sideslip flow correction was then plotted against either the average measured angle of attack or the average measured angle of sideslip.

To look at the effect of the sideslip angle on the angle-of-sideslip flow correction, that flow correction was plotted against the measured angle of attack for three values of sideslip. As the model was sideslipped, the angle-of-sideslip flow correction increased at one sensor location and decreased at the other. Thus, the average angle-of-sideslip flow correction from the left and right sensors did not change very much as the model was sideslipped. In order to present the effect of the sideslip angle, the angle-of-sideslip flow correction from the left sensor was plotted against the measured angle of attack from the left sensor. Data from the left sensor were used because these data were more consistent than the data from the right sensor.

Rotary Wind-Tunnel Tests

The research airplane was found to spin with an average spin coefficient of about 0.3. Therefore, data from the rotary wind-tunnel tests for rates of rotation of $\Omega b/2V_T = \pm 0.3$ were used over an angle-of-attack range from 8° to 90°. While the model was rotating, the angle of attack at each wingtip was measured by a flow direction sensor and these measurements were averaged to obtain a measured angle of attack at the center of gravity of the model. Next, the measured

angles of attack at the c.g. were averaged when the model was rotating to both the right and left. This averaged measured angle of attack of the model was then compared with the true angle of attack of the model to determine the flow correction.

Level Flight Tests

The research airplane was flown in steady, straight and level flight at which time the true angle of attack was determined. In level flight, the flight path angle γ was 0. So, from the equation

$$\theta = \alpha + \gamma \tag{10}$$

it can be seen that for level flight the true angle of attack equaled the pitch angle θ. The pitch angle was simply the angle at which the X body axis was inclined to the horizon, and it was found by taking the inverse sine of the longitudinal acceleration. Thus,

$$\alpha_t = \theta = \sin^{-1} a_x \tag{11}$$

Once the true angle of attack was known, it was subtracted from the measured angle of attack to determine the flow correction. Finally, the flow correction was plotted against the measured angle of attack to determine the characteristics of the flow correction at low angles of attack.

Spin Flight Tests

Three methods have been used to calculate the true angle of attack of an airplane in spinning flight. Two methods have been previously proposed, and the other method is an extension of an existing technique. Two methods make assumptions that are typically not valid for spinning flight and, thus, their value is questionable. However, since these two methods are still being used, results of these methods have been shown to enable comparison with the wind-tunnel data and a more rigorous method.

Method 1. After the research airplane had been in a spin for six or more turns, most of the measured quantities became reasonably constant with time. By the time that the spin became steady, the velocity vector had become nearly vertical. For this method, the airplane velocity vector was assumed to be oriented along the angular-velocity vector. This meant that the spin axis passed through the center of gravity of the airplane. This assumption implies that the airplane could not have a spin radius and, thus, its center of gravity could not move in a helical path.

Once this assumption was made, the airplane angular-velocity vector could be transferred from the wind axis system to the body axis system to give equations for the angular rates as functions of the flow angles. With these expressions the angular rates measured during the steady part of the spin were used to determine the true angles of attack and sideslip of the airplane in the spin.

Finally, the measured angles of attack and sideslip were transferred to the center of gravity of the airplane, as shown in appendix A. These measured angles of attack and sideslip at the c.g. were compared with the true angles of attack and sideslip calculated from this method to determine the angle-of-attack and angle-of-sideslip flow corrections. The details of method 1 are presented in appendix B.

Method 2. This method utilized the fact that once the airplane was in a steady spin it was not accelerating; therefore, the sum of the forces acting on the airplane in the vertical direction had to be 0. This meant that the aerodynamic force in the vertical direction was equal and opposite to the gravity force acting on the body. Since the linear accelerometers measured the aerodynamic forces acting on the airplane, these body axis accelerations were resolved to yield the aerodynamic force along the velocity vector. It was then assumed that the velocity vector was aligned with the gravity vector. This meant that the spin axis passed through the center of gravity of the airplane (i.e., that the spin radius was 0). Thus, the center of gravity of the airplane moved downward along the gravity vector instead of moving around the spin axis in a helical path. So, for equilibrium, the aerodynamic force along the velocity vector had to be equal and opposite to the gravity force. By using this relation and the measured linear accelerations, the true angle of attack of the airplane could be determined. Once the measured angles of attack at the sensors were transformed to the c.g., the flow correction could be determined. The specifics of this method are shown in appendix C.

Method 3. A method to calculate the flow direction angles during a steady spin was proposed in reference 19. This method was less restrictive than the previous two methods in that it did not require the spin axis to pass through the center of gravity of the airplane. The method used the measured linear accelerations, angular rates, and vertical velocity to compute the flow direction angles of the airplane during the spin. Since some of the data were measured in the body axes and other data were measured in the ground axes, a relationship between the two sets of axes was determined. The direction of the flight path could then be transferred from the ground axes to the body axes and expressed

in terms of the true angle of attack and true angle of sideslip. The measured angles of attack and sideslip were transformed to the c.g., as indicated in appendix A. Finally, the measured and the calculated or true angles of attack and sideslip were compared to determine the flow correction. Method 3 has been rederived in appendix D.

Results and Discussion

Static Wind-Tunnel Tests

Force and moment data. The longitudinal force and moment characteristics of the basic model are shown in figure 13. At the relatively low Reynolds number of these tests, the lift curve reaches a maximum value at an angle of attack of 12°. The resultant-force coefficient is a combination of the lift and drag coefficients. It exhibits the decrease in lift after the stall as well as the large rise in the drag coefficient at the larger angles of attack. The pitching-moment coefficient shows that the configuration, with the tails removed, is unstable up to the stall angle of attack as expected.

Figure 14 compares the lift coefficient data for the basic configuration with that for the configurations with the outboard and full-span leading-edge droop modifications. When compared with the basic configuration, the configuration with the outboard droop modification exhibits similar stall characteristics but increased lift in the middle of the angle-of-attack range. The full-span leading-edge droop modification increases the maximum lift coefficient attainable, the stall angle of attack, and the lift in the middle of the angle-of-attack range.

Basic angle-of-attack flow correction. The true angle of attack plotted against the measured angle of attack for the basic model at zero sideslip is shown in figure 15. The flow correction is the difference between the data and the $\alpha_t = \alpha_m$ line. Figure 16 shows the flow correction plotted against the measured angle of attack. The data show a reduction in the flow correction after the stall angle of attack. This reduction is probably due to the loss of circulation on the wing after the stall. At an angle of attack of about 20°, the flow correction starts to increase again. This increase occurs at almost the same angle of attack as that at which the lift coefficient begins increasing again. The flow correction reaches a maximum of about 13° at a measured angle of attack of about 95°. It appears that the flow correction is dependent on the drag as well as on the lift because the general shape of the flow correction curve resembles the shape of the resultant-force coefficient shown in figure 13.

From this flow correction data it may be seen that for the model at a flat spin attitude (at an angle of attack near 90°), using the measured angle of attack instead of the true angle of attack results in an error of about 15 percent.

Effect of wing-configuration changes. During the course of the stall/spin program, many wing modifications were evaluated as to the degree of spin resistance they provided. Also, the effect of the controls on the spin entry, developed spin, and recovery was evaluated. Either the addition of modifications to the wing or the deflection of the ailerons will change the flow over the wing and, therefore, can possibly change the flow correction. A number of tests were made to evaluate the effect of wing modifications and aileron deflections on the flow correction.

The effect on the flow correction of adding the outboard droop to the wing is shown in figure 17. The modification increases the flow correction slightly between measured angles of attack of 15° and 35°. This may be due to the fact that the wing with the outboard droop modification produces a larger lift coefficient than the basic unmodified wing over this angle-of-attack range. This increased lift would cause increased upwash at the sensor location, which would increase the flow correction.

Adding the full-span droop to the model affects the flow correction, as shown in figure 18. Again, the flow correction is increased between angles of attack of 15° and 35°. This increase may also be attributed to the larger lift coefficient produced by the wing with the full-span droop over this angle-of-attack range.

The effect of aileron deflection on the flow correction is shown in figure 19. In order to average the data from the right and left sensors, two wind-tunnel runs were conducted, one with both ailerons deflected down and the other with both ailerons deflected up. A full-down deflection of both ailerons slightly increases the flow correction, whereas a full-up deflection of both ailerons slightly decreases the flow correction. This change in the flow correction is related to the change in lift and drag on the wing caused by deflection of the ailerons. To apply this correction to the case in which the ailerons are fully deflected, the "up" correction would be applied to the angle of attack measured in front of the wing with the aileron deflected up, and the "down" correction would be applied to the angle of attack measured in front of the wing with the aileron deflected down.

Both leading-edge modifications and aileron deflections seemed to change the flow correction. However, the differences were never larger than ±1° and often much less. These differences were within the repeatability of the angle-of-attack measurements.

Therefore, the basic correction from figure 16 could be used to correct measured angle-of-attack data, even when a leading-edge modification was added to the wing or when the ailerons were deflected.

Effect of angle of sideslip. The effect of the angle of sideslip on the angle-of-attack flow correction was also investigated. Figure 20 shows the flow correction as a function of the measured angle of attack for the right flow direction sensor. At angles of attack larger than 50°, the flow correction is reduced for positive angles of sideslip and is increased for negative angles of sideslip. It is possible that this result is due to increased lift at the right wingtip for negative sideslip angles and decreased lift for positive sideslip angles.

Basic angle-of-sideslip flow correction.. The flow correction to be applied to the angle-of-sideslip measurements for the basic model is shown in figure 21 as a function of the average measured angle of attack. This figure shows that the sideslip flow correction is also significant. The correction reaches a maximum of about 7° at the large measured angles of attack. This means that at the sensor location the local flow is skewed outboard by up to 7° at each wingtip. To correct the measured sideslip angles, the average angle-of-sideslip flow correction presented in figure 21 should be added to the measured sideslip angle at the right sensor and subtracted from the measured sideslip angle at the left sensor.

Effect of full-span droop modification. The effect on the sideslip flow correction of adding the full-span leading-edge droop modification to the model is shown in figure 22. The main difference is that the addition of the wing modification reduces the sideslip flow correction over an angle-of-attack range from 15° to 55°. The model has more lift in this angle-of-attack range with the leading-edge modification on the wing. This increases the wing loading and may tend to reduce the spanwise flow, thus reducing the sideslip flow correction in this region.

Effect of angle of sideslip. Figure 23 shows the effect of the angle of sideslip on the angle-of-sideslip flow correction as a function of the measured angle of attack for the left flow direction sensor. At the large angles of attack, the sideslip flow correction at the left sensor is reduced for positive angles of sideslip and increased for negative angles of sideslip. As was indicated earlier, a positive sideslip angle may increase the lift at the trailing wing (the left wing) whereas a negative sideslip angle may decrease the lift at the leading wing (the left wing). An increase in lift at the wingtip may reduce the spanwise flow and thus reduce the angle-of-sideslip flow correction for positive sideslip angles, as shown in figure 23.

Effect of angle of attack. The variation of the angle-of-sideslip flow correction with the measured angle of sideslip, for different angles of attack, is shown in figure 24. At low angles of attack the sideslip flow correction is basically unchanged by the angle of sideslip. However, at larger angles of attack, the sideslip flow correction exhibits a strong dependence on the sideslip angle. Again, it can be seen that the sideslip flow correction increases with the angle of attack.

Rotary Wind-Tunnel Tests

The previous section presented the results of the flow correction determined by static wind-tunnel tests. This flow correction could be applied to angle-of-attack data measured onboard an airplane during a spin. Since the spin is a rotational flight condition, however, it is possible that a statically determined flow correction would not be adequate in this situation. To determine if the static correction could be used, the effect of rotation on the flow correction was investigated. For this investigation the rotary-balance apparatus in the Langley Spin Tunnel was used. Figure 25 compares this rotary data with the static flow correction obtained in the Spin Tunnel. The two sets of data agree fairly well, and thus it appears that the presence of rotation does not affect the statically determined flow correction.

Level Flight Tests

The airplane was flown in steady, straight and level flight to determine a low-angle-of-attack flow correction. Since these data were not available for the basic airplane, data taken with the outboard droop modification on the wing were used. Figure 26 shows the comparison of the static wind-tunnel data to the low-angle-of-attack flight data. It can be seen that the wind-tunnel and flight data are in general agreement in this angle-of-attack range.

Spin Flight Tests

Data from 15 steady spins were analyzed using the three methods described in appendixes B to D. Some spins with different leading-edge modifications were used in order that different spin modes could be found to cover a range of measured angles of attack. Data were also used from spins in which the rockets were fired in a prospin direction to obtain spin modes at large angles of attack. The 15 steady

spins covered an angle-of-attack range from 33° to 91°. Method 3 was applied to two spirals in which the angle of attack was below 30°. About 40 percent of the spins analyzed were left spins. In general, data are shown for the spins for which each method worked the best. However, in order to show data over a large angle-of-attack range, some data are shown in which the method did not work as well as was hoped.

Figure 27 compares the results of the three methods used to analyze the spin flight data with the static wind-tunnel data. The results of methods 1 and 2 each applied to eight spins are shown by the figure. Method 1 used the measured angular rates of the airplane to determine the true angle of attack of the airplane, whereas method 2 used the measured linear accelerations. Figure 27 also shows the results of method 3 applied to seven spins and two spirals. Method 3 used both the measured angular rates and linear accelerations as well as the vertical velocity to calculate the true angle of attack of the airplane.

In general, methods 1 and 3 usually underestimated the angle-of-attack flow correction, whereas method 2 usually overestimated the flow correction. For the data shown in figure 27, statistical analysis showed that the results of method 3 agreed with the model flow corrections better than did the results of methods 1 and 2, and that methods 1 and 2 agreed about the same. For all the data analyzed, statistical analysis showed that method 3 had a standard deviation about 7.5 percent lower than that of method 1. Overall, method 2 did much worse than both methods 1 and 3. The fact that method 3 gave the best agreement may be attributed to the fact that, unlike methods 1 and 2, method 3 does not require the spin axis to pass through the center of gravity of the airplane.

Methods 1 and 3 did not produce conclusive results for the sideslip angle during the spin; therefore, no angle-of-sideslip flow correction data are presented. In general, both methods indicated the general trends shown by the wind-tunnel data; however, there was an offset between the sideslip flow correction determined in flight and the correction measured in the wind tunnel.

Although there is some scatter in the flow correction determined by these three methods, the methods do indicate the trends and magnitude of the static wind-tunnel data. Thus, if no wind-tunnel data are available, these methods could be used to get an estimate of the angle-of-attack flow correction.

Summary of Results

An investigation has been conducted into the nature of corrections for flow direction measurements obtained with wingtip-mounted sensors. Corrections to be applied to the angles of attack and sideslip, measured by sensors mounted in front of each wingtip of a general aviation airplane, have been determined. These flow corrections have been obtained from both wind-tunnel and flight tests over an angle-of-attack range from 0° to 85°. The effects of flow parameters and configuration modifications on the angle-of-attack and angle-of-sideslip flow corrections have been determined. However, the wind-tunnel tests were conducted at a low Reynolds number and these general aviation configurations have a known sensitivity to Reynolds number. Therefore, the wind-tunnel-determined flow correction can be used to provide only an approximate estimate of the true angle of attack of a full-scale airplane. The results of this investigation may be summarized as follows:

1. The flow corrections to be applied to both the measured angle of attack and measured angle of sideslip were found to be substantial.

2. The angle-of-attack flow correction appears to be a function of the longitudinal aerodynamic forces acting on the model.

3. The effects of wing configuration changes on the angle-of-attack flow correction were found to be small.

4. The angle of sideslip had a significant effect on both the angle-of-attack and angle-of-sideslip flow corrections at large angles of attack.

5. The presence of spinning rotation did not appreciably alter the angle-of-attack flow correction.

6. The angle-of-attack flow correction determined from the static wind-tunnel tests was in agreement with the correction determined in level flight.

7. The best results were given by the least restrictive of the three analytical methods used to determine the flow correction during steady spins.

8. If wind-tunnel data are not available, it would be preferable to use results from any of the three methods to estimate the angle-of-attack flow correction in a spin than not to apply a correction at all.

NASA Langley Research Center
Hampton, VA 23665-5225
June 7, 1985

Appendix A

Transferring Measurements to the Center of Gravity

The flow direction and velocity sensors measured the angles of attack and sideslip and the true airspeed in front of each of the wingtips. During a spin, these measurements were different from each other and different from the velocity and the angles of attack and sideslip that the c.g. of the airplane was experiencing. So in order to determine the velocity and the angles of attack and sideslip of the airplane, the sensor measurements were transferred to the c.g. of the airplane.

In transferring these measurements, the flow direction and velocity sensor readings were first converted to body velocity components at the sensors. Thus,

$$\left.\begin{aligned} u_s(i) &= V_{T,m}(i) \cdot \cos\alpha_m(i) \cdot \cos\beta_m(i) \\ v_s(i) &= V_{T,m}(i) \cdot \sin\beta_m(i) \\ w_s(i) &= V_{T,m}(i) \cdot \sin\alpha_m(i) \cdot \cos\beta_m(i) \end{aligned}\right\} \tag{A1}$$

where (i) denotes either right or left.

The body velocities at the sensor were transferred to the center-of-gravity location by using the corrections for vehicle rotation as follows:

$$\left.\begin{aligned} u_{cg}(i) &= u_s(i) + r \cdot y(i) - q \cdot z(i) \\ v_{cg}(i) &= v_s(i) + p \cdot z(i) - r \cdot x(i) \\ w_{cg}(i) &= w_s(i) + q \cdot x(i) - p \cdot y(i) \end{aligned}\right\} \tag{A2}$$

The body velocities at the center-of-gravity location were then averaged as follows:

$$\left.\begin{aligned} u_{cg} &= \frac{u_{cg}(L) + u_{cg}(R)}{2} \\ v_{cg} &= \frac{v_{cg}(L) + v_{cg}(R)}{2} \\ w_{cg} &= \frac{w_{cg}(L) + w_{cg}(R)}{2} \end{aligned}\right\} \tag{A3}$$

where L and R denote left and right, respectively.

Finally, these averaged body axis velocities were reconstructed into the desired quantities at the c.g. of the airplane:

$$\alpha_{m,cg} = \tan^{-1}(w_{cg}/u_{cg}) \tag{A4}$$

$$V_{T,m,cg} = (u_{cg}^2 + v_{cg}^2 + w_{cg}^2)^{1/2} \tag{A5}$$

$$\beta_{m,cg} = \sin^{-1}(v_{cg}/V_{T,m,cg}) \tag{A6}$$

Appendix B

Calculation of Angles of Attack and Sideslip Using Method 1

Method 1 used the angular rates of the airplane to determine the true angles of attack and sideslip of the airplane during a steady spin. It was assumed that the airplane velocity vector was oriented along the angular-velocity vector. This assumption made it possible to transfer the airplane angular-velocity vector from the wind axis system to the body axis system, as indicated in reference 20. Thus,

$$\boldsymbol{\Omega}_b = \mathbf{L}_{bw}\boldsymbol{\Omega}_w \tag{B1}$$

$$\begin{Bmatrix} p \\ q \\ r \end{Bmatrix} = \begin{bmatrix} \cos\alpha_t \cos\beta_t & -\cos\alpha_t \sin\beta_t & -\sin\alpha_t \\ \sin\beta_t & \cos\beta_t & 0 \\ \sin\alpha_t \cos\beta_t & -\sin\alpha_t \sin\beta_t & \cos\alpha_t \end{bmatrix} \begin{Bmatrix} \Omega \\ 0 \\ 0 \end{Bmatrix} \tag{B2}$$

$$p = \Omega \cos\alpha_t \cos\beta_t \tag{B3}$$

$$q = \Omega \sin\beta_t \tag{B4}$$

$$r = \Omega \sin\alpha_t \cos\beta_t \tag{B5}$$

Equations (B3) and (B5) were combined to give the true angle of attack at the center of gravity of the airplane in a steady spin:

$$\alpha_{t,\mathrm{cg}} = \tan^{-1}(r/p) \tag{B6}$$

The equations for the angular rates could also be used to compute a true angle of sideslip at the center of gravity of the airplane in a steady spin. Equations (B3) and (B4) were combined to yield:

$$\beta_{t,\mathrm{cg}} = \tan^{-1}\left(\frac{q \cdot \cos\ \alpha_{t,\mathrm{cg}}}{p}\right) \tag{B7}$$

Appendix C

Calculation of Angle of Attack Using Method 2

Method 2 used the linear accelerations of the airplane to determine the true angle of attack of the airplane during a steady spin. Because the airplane was in equilibrium during a steady spin, the sum of the forces acting on the airplane in any particular direction had to be 0. It was assumed that the velocity vector was aligned with the gravity vector. So for equilibrium, the aerodynamic force along the velocity vector had to be equal and opposite to the gravity force acting on the airplane. Thus,

$$F_w = -F_g \tag{C1}$$

where

$$F_w = ma_w$$

$$F_g = mg$$

The body-axis accelerations were resolved, as indicated in reference 12, to yield an acceleration along the velocity vector:

$$a_w = g[(a_x \cos \alpha_t + a_z \sin \alpha_t) \cos \beta + a_y \sin \beta] \tag{C2}$$

Therefore,

$$ma_w = -mg$$

$$mg[(a_x \cos \alpha_t + a_z \sin \alpha_t) \cos \beta + a_y \sin \beta] = -mg \tag{C3}$$

Then,

$$(a_x \cos \alpha_t + a_z \sin \alpha_t) \cos \beta + a_y \sin \beta = -1$$

$$a_x \cos \alpha_t + a_z \sin \alpha_t = -(1 + a_y \sin \beta)/\cos \beta$$

Let

$$C = (1 + a_y \sin \beta)/\cos \beta \tag{C4}$$

Then,

$$a_z \sin \alpha_t = -a_x \cos \alpha_t - C$$

$$a_z^2 \sin^2 \alpha_t = a_x^2 \cos^2 \alpha_t + 2a_x C \cos \alpha_t + C^2$$

$$a_z^2 - a_z^2 \cos^2 \alpha_t = a_x^2 \cos^2 \alpha_t + 2a_x C \cos \alpha_t + C^2$$

$$(a_x^2 + a_z^2) \cos^2 \alpha_t + 2a_x C \cos \alpha_t + C^2 - a_z^2 = 0 \tag{C5}$$

Therefore,

$$\cos \alpha_t = \frac{-2a_x C \pm \sqrt{4a_x^2 C^2 - 4\left(a_x^2 + a_z^2\right)\left(C^2 - a_z^2\right)}}{2\left(a_x^2 + a_z^2\right)}$$

$$\cos \alpha_t = \frac{-a_x C \pm \sqrt{a_x^2 C^2 - a_x^2 C^2 - a_z^2 C^2 + a_x^2 a_z^2 + a_z^4}}{a_x^2 + a_z^2}$$

$$\cos \alpha_t = \frac{-a_x C \pm a_z \sqrt{a_x^2 + a_z^2 - C^2}}{a_x^2 + a_z^2} \tag{C6}$$

where the negative sign gives the desired root. Then,

$$\alpha_t = \cos^{-1}\left(\frac{-a_x C - a_z \sqrt{a_x^2 + a_z^2 - C^2}}{a_x^2 + a_z^2}\right) \tag{C7}$$

Appendix D

Calculation of Angles of Attack and Sideslip Using Method 3

A set of relations may be developed that can be used to calculate the angles of attack and sideslip of an airplane in a steady spin. Method 3 was proposed in reference 19 and is rederived here in a more complete manner. This method utilizes the linear accelerations, angular rates, and the vertical velocity to compute the true angles of attack and sideslip at the center-of-gravity location of the airplane.

Because some of the measurements are made with respect to the airplane body axes (the linear accelerations and angular rates) and others with respect to the ground axes (the vertical velocity), the relationship between the two axis systems must be determined.

The ground axis system has its origin at the center-of-gravity location of the airplane. The Z_g-axis points vertically downward and is aligned with the gravity vector. The X_g-axis is in the horizontal plane and points through the spin axis. The Y_g-axis is in the horizontal plane and is mutually perpendicular to the X_g- and Z_g-axes. The ground axis systems turn with the center-of-gravity location of the airplane as the airplane travels in a helical path about the spin axis. Figure 28 shows an instantaneous arrangement of the ground axis system.

The angular velocity of the airplane about the spin axis in the body axis system may be determined from the body angular rates as

$$\boldsymbol{\Omega} = p\mathbf{i} + q\mathbf{j} + r\mathbf{k}$$

$$|\boldsymbol{\Omega}| = (p^2 + q^2 + r^2)^{1/2}$$

However, the spin axis is vertical in the ground axis system; thus,

$$\boldsymbol{\Omega} = |\boldsymbol{\Omega}|\mathbf{K}$$

For an equilibrium spin, the resultant-force or resultant-acceleration vector must be located in the X_gZ_g-plane. Figure 29 shows the relationship between the resultant-acceleration and resultant-rotation vectors. The resultant acceleration may be determined by the measured body linear accelerations:

$$\mathbf{A} = a_x\mathbf{i} + a_y\mathbf{j} + a_z\mathbf{k}$$

By using the law of cosines, the angle between the resultant-acceleration and resultant-rotation vectors may be found as follows:

$$|\mathbf{A} - \boldsymbol{\Omega}|^2 = |\mathbf{A}|^2 + |\boldsymbol{\Omega}|^2 - 2|\mathbf{A}| \cdot |\boldsymbol{\Omega}| \cos\ \sigma$$

$$(\mathbf{A} - \boldsymbol{\Omega}) \cdot (\mathbf{A} - \boldsymbol{\Omega}) = \mathbf{A} \cdot \mathbf{A} + \boldsymbol{\Omega} \cdot \boldsymbol{\Omega} - 2|\mathbf{A}| \cdot |\boldsymbol{\Omega}| \cos\ \sigma$$

$$\mathbf{A} \cdot \mathbf{A} - \mathbf{A} \cdot \boldsymbol{\Omega} - \mathbf{A} \cdot \boldsymbol{\Omega} + \boldsymbol{\Omega} \cdot \boldsymbol{\Omega} = \mathbf{A} \cdot \mathbf{A} + \boldsymbol{\Omega} \cdot \boldsymbol{\Omega} - 2|\mathbf{A}| \cdot |\boldsymbol{\Omega}| \cos\ \sigma$$

$$2\mathbf{A} \cdot \boldsymbol{\Omega} = 2|\mathbf{A}| \cdot |\boldsymbol{\Omega}| \cos\ \sigma$$

$$\cos\ \sigma = \frac{\mathbf{A} \cdot \boldsymbol{\Omega}}{|\mathbf{A}| \cdot |\boldsymbol{\Omega}|}$$

$$\cos\ \sigma = \frac{a_x p + a_y q + a_z r}{|\mathbf{A}| \cdot |\boldsymbol{\Omega}|}$$

Once σ is known, the resultant-acceleration vector can be transferred into the ground axis system. Thus,

$$|\mathbf{A}_X| = |\mathbf{A}| \sin\ \sigma$$

$$|\mathbf{A}_Z| = |\mathbf{A}| \cos\ \sigma$$

Since the airplane is in equilibrium, the aerodynamic acceleration in the vertical direction must be equal and opposite to the acceleration of gravity. In other words,

$$|\mathbf{A}_Z| = 1g$$

The center of gravity of the airplane exhibits a circular motion in the X_gY_g-plane; thus, the velocity in this plane is in the Y_g-direction only (i.e., $U = 0$). Also, the aerodynamic acceleration in the X_g-direction must be equal to the centrifugal acceleration in order for the airplane to be in equilibrium. Thus,

$$|\mathbf{A}_X|g = A_c$$

$$A_c = \frac{V_T^2}{R_S}$$

$$V_T = |\boldsymbol{\Omega}|R_S$$

$$A_c = \frac{|\boldsymbol{\Omega}|^2 R_S^2}{R_S} = |\mathbf{A}_X|g$$

$$R_S = \frac{|\mathbf{A}_X|g}{|\boldsymbol{\Omega}|^2}$$

$$A_c = \frac{V_T|\boldsymbol{\Omega}|R_S}{R_S} = |A_X|g$$

$$V_T|\boldsymbol{\Omega}| = |A_X|g$$

$$V_T = \frac{|\mathbf{A}_X|g}{|\boldsymbol{\Omega}|}$$

$$|\mathbf{V}_T| = (U^2 + V^2 + W^2)^{1/2}$$

$$W = -\dot{h} \qquad U = 0$$

$$|\mathbf{V}_T| = [V^2 + (-\dot{h})^2]^{1/2}$$

$$\delta = \tan^{-1}\left(V/-\dot{h}\right)$$

Next, we define a vector $\mathbf{X}'_g$ that is parallel to the X_g-axis and intersects the resultant-acceleration vector at unit distance from origin (fig. 29):

$$\mathbf{X}'_g = \frac{\mathbf{A}}{|\mathbf{A}|} - \cos\ \sigma \frac{\Omega}{|\boldsymbol{\Omega}|}$$

The direction components of $\mathbf{X}'_g$ in the body axes are

$$i = \frac{a_x}{|\mathbf{A}|} - \cos\ \sigma \frac{p}{|\boldsymbol{\Omega}|}$$

$$j = \frac{a_y}{|\mathbf{A}|} - \cos\ \sigma \frac{q}{|\boldsymbol{\Omega}|}$$

$$k = \frac{a_z}{|\mathbf{A}|} - \cos\ \sigma \frac{r}{|\boldsymbol{\Omega}|}$$

$$|\mathbf{X}'_g| = \left(|i|^2 + |j|^2 + |k|^2\right)^{1/2}$$

The Y_g-axis is mutually perpendicular to the $\mathbf{X}_g$- and Z_g-axes and its direction may be found by the definition of orthogonality:

$$\mathbf{I} \cdot \mathbf{J} = 0$$

$$\mathbf{J} \cdot \mathbf{J} = 1$$

$$\mathbf{K} \cdot \mathbf{J} = 0$$

The direction cosines of the Y_g-axis in the body axes are found by the solution of the following direction cosine equation:

$$\begin{bmatrix} \ell_X & m_X & n_X \\ \ell_Y & m_Y & n_Y \\ \ell_Z & m_Z & n_Z \end{bmatrix} \begin{Bmatrix} \ell_Y \\ m_Y \\ n_Y \end{Bmatrix} = \begin{Bmatrix} 0 \\ 1 \\ 0 \end{Bmatrix}$$

Using Cramer's rule of determinants gives

$$\ell_Y = -\begin{vmatrix} m_X & n_X \\ m_Z & n_Z \end{vmatrix} = m_Z n_X - m_X n_Z$$

or

$$\ell_Y = \frac{q}{|\boldsymbol{\Omega}|}\frac{k}{|\mathbf{X}'_g|} - \frac{j}{|\mathbf{X}'_g|}\frac{r}{|\boldsymbol{\Omega}|}$$

$$m_Y = \begin{vmatrix} \ell_X & n_X \\ \ell_Z & n_Z \end{vmatrix} = \ell_X n_Z - \ell_Z n_X$$

or

$$m_Y = \frac{i}{|\mathbf{X}'_g|}\frac{r}{|\boldsymbol{\Omega}|} - \frac{p}{|\boldsymbol{\Omega}|}\frac{k}{|\mathbf{X}'_g|}$$

and

$$n_Y = -\begin{vmatrix} \ell_X & m_X \\ \ell_Z & m_Z \end{vmatrix} = \ell_Z m_X - \ell_X m_Z$$

or

$$n_Y = \frac{p}{|\boldsymbol{\Omega}|}\frac{j}{|\mathbf{X}'_g|} - \frac{i}{|\mathbf{X}'_g|}\frac{q}{|\boldsymbol{\Omega}|}$$

Next, the direction cosines in the ground axis system are determined. The direction cosines of the flight path are

$$\ell'_v = 0$$

$$m'_v = \pm \sin\ \delta = \frac{\pm V}{|\mathbf{V}_T|} \qquad \begin{pmatrix} -, \text{ right spins;} \\ +, \text{ left spins} \end{pmatrix}$$

$$n'_v = \cos\ \delta = -\dot{h}/|\mathbf{V}_T|$$

The direction cosines of the Y_b body axis are

$$\ell'_y = m_X$$

$$m'_y = m_Y$$

$$n'_y = \pm m_Z \qquad \begin{pmatrix} +, \text{ right spins;} \\ -, \text{ left spins} \end{pmatrix}$$

The direction cosines of the X_b body axis are

$$\ell'_x = \ell_X$$

$$m'_x = \ell_Y$$

$$n'_x = \pm \ell_Z \qquad \begin{pmatrix} +, \text{ right spins;} \\ -, \text{ left spins} \end{pmatrix}$$

The relationship between a line and a plane is used to find the ground flight path components in the body system of axes. Thus,

$$\sin \beta_t = \frac{v}{|\mathbf{V}_T|} = \ell'_v \ell'_y + m'_v m'_y + n'_v n'_y$$

$$\sin \beta_t = \pm \sin \delta \left(\frac{i}{|\mathbf{X}'_g|} \frac{r}{|\boldsymbol{\Omega}|} - \frac{p}{|\boldsymbol{\Omega}|} \frac{k}{|\mathbf{X}'_g|} \right) + \cos \delta \left(\frac{\pm q}{|\boldsymbol{\Omega}|} \right)$$

$$\beta_t = \sin^{-1} \left[\frac{\pm V}{|\mathbf{V}_T|} \left(\frac{i}{|\mathbf{X}'_g|} \frac{r}{|\boldsymbol{\Omega}|} - \frac{p}{|\boldsymbol{\Omega}|} \frac{k}{|\mathbf{X}'_g|} \right) + \frac{-\dot{h}}{|\mathbf{V}_T|} \frac{\pm q}{|\boldsymbol{\Omega}|} \right]$$

$$\cos \mu = \frac{u}{|\mathbf{V}_T|} = \ell'_v \ell'_x + m'_v m'_x + n'_v n'_x$$

$$\cos \mu = \frac{\pm V}{|\mathbf{V}_T|} \left(\frac{q}{|\boldsymbol{\Omega}|} \frac{k}{|\mathbf{X}'_g|} - \frac{j}{|\mathbf{X}'_g|} \frac{r}{|\boldsymbol{\Omega}|} \right) + \frac{-\dot{h}}{|\mathbf{V}_T|} \frac{\pm p}{|\boldsymbol{\Omega}|}$$

$$\cos \beta_t = (u^2 + w^2)^{1/2} / |\mathbf{V}_T|$$

$$\cos \alpha_t = u / (u^2 + w^2)^{1/2}$$

$$\cos \alpha_t = \cos \mu / \cos \beta_t$$

$$\alpha_t = \cos^{-1} (\cos \mu / \cos \beta_t)$$

References

1. Kershner, David D.: *Miniature Flow-Direction and Airspeed Sensor for Airplanes and Radio-Controlled Models in Spin Studies.* NASA TP-1467, 1979.
2. Alford, William J., Jr.: *Theoretical and Experimental Investigation of the Subsonic-Flow Fields Beneath Swept and Unswept Wings With Tables of Vortex-Induced Velocities.* NACA Rep. 1327, 1957. (Supersedes NACA TN 3738.)
3. Sliwa, Steven Mark: A Study of Data Extraction Techniques for Use in General Aviation Aircraft Spin Research. M.S. Thesis, George Washington Univ., Sept. 1978.
4. Gracey, William: *Summary of Methods of Measuring Angle of Attack on Aircraft.* NACA TN 4351, 1958.
5. Ribner, Herbert S.: *Notes on the Propeller and Slipstream in Relation to Stability.* NACA WR L-25, 1944. (Formerly NACA ARR L4I12a.)
6. Milne-Thomson, L. M.: *Theoretical Aerodynamics, Fourth ed.* Dover Publ., Inc., c.1958.
7. Bowman, James S., Jr.; Stough, Harry P.; Burk, Sanger M., Jr.; and Patton, James M., Jr.: Correlation of Model and Airplane Spin Characteristics for a Low-Wing General Aviation Research Airplane. AIAA Paper 78-1477, Aug. 1978.
8. Moul, Thomas M.: *Wind-Tunnel Investigation of the Flow Correction for a Model-Mounted Angle of Attack Sensor at Angles of Attack From $-10°$ to $110°$.* NASA TM-80189, 1979.
9. Moul, Thomas M.; and Taylor, Lawrence W., Jr.: Determination of an Angle of Attack Sensor Correction for a General Aviation Airplane at Large Angles of Attack as Determined From Wind Tunnel and Flight Tests. AIAA-80-1845, Aug. 1980.
10. Moul, Thomas Martin: Determination of Corrections to Flow Direction Measurements Obtained With a Wing-Tip Mounted Sensor. M.S. Thesis, George Washington Univ., Aug. 1983.
11. Mechtly, E. A.: *The International System of Units—Physical Constants and Conversion Factors (Second Revision).* NASA SP-7012, 1973.
12. Gainer, Thomas G.; and Hoffman, Sherwood: *Summary of Transformation Equations and Equations of Motion Used in Free-Flight and Wind-Tunnel Data Reduction and Analysis.* NASA SP-3070, 1972.
13. Staff of Langley Research Center: *Exploratory Study of the Effects of Wing-Leading-Edge Modifications on the Stall/Spin Behavior of a Light General Aviation Airplane.* NASA TP-1589, 1979.
14. O'Bryan, Thomas C.; Goode, Maxwell W.; Gregory, Frederick D.; and Mayo, Marna H.: *Description of an Experimental (Hydrogen Peroxide) Rocket System and Its Use in Measuring Aileron and Rudder Effectiveness of a Light Airplane.* NASA TP-1647, 1980.
15. Mulcay, William J.; and Rose, Robert A.: *Rotary Balance Data for a Typical Single-Engine General Aviation Design for an Angle-of-Attack Range of $8°$ to $90°$. I—Low-Wing Model C.* NASA CR-3200, 1980.
16. O'Bryan, Thomas C.; Edwards, Thomas E.; and Glover, Kenneth E.: Some Results From the Use of a Control Augmentation System To Study the Developed Spin of a Light Plane. AIAA Paper 79-1790, Aug. 1979.
17. Chambers, Joseph R.: Overview of Stall/Spin Technology. AIAA-80-1580, Aug. 1980.
18. Hoerner, Sighard F.; and Borst, Henry V.: *Fluid-Dynamic Lift.* Hoerner Fluid Dynamics (Brick Town, N.J.), c.1975.
19. Soulé, Hartley A.; and Scudder, Nathan F.: *A Method of Flight Measurement of Spins.* NACA Rep. 377, 1931.
20. Etkin, Bernard: *Dynamics of Atmospheric Flight.* John Wiley & Sons, Inc., c.1972.

TABLE I. CHARACTERISTICS OF RESEARCH AIRPLANE

Airplane:	
Maximum gross mass (normal category), kg (lbm)	1111.30 (2450)
Engine power, kW (hp)	134.23 (180)
Propeller diameter, m (ft)	1.93 (6.33)
Length, m (ft)	7.84 (25.73)
Height, m (ft)	2.50 (8.20)
Wing:	
Airfoil	NACA 63_2A415
Span, m (ft)	9.98 (32.75)
Area, m^2 (ft^2)	13.56 (146)
Chord, m (ft)	1.34 (4.39)
Mean aerodynamic chord, m (ft)	1.34 (4.39)
Aspect ratio	7.35
Dihedral, deg	6.5
Aileron span, m (ft)	1.64 (5.38)
Aileron area (each), m^2 (ft^2)	0.64 (6.93)
Aileron chord, m (ft)	0.39 (1.29)
Vertical tail:	
Airfoil	Modified NACA 63_1A012
Area, m^2 (ft^2)	1.36 (14.6)
Rudder area, m^2 (ft^2)	0.43 (4.62)
Length (quarter chord of wing to quarter chord of vertical tail), m (ft)	4.14 (13.6)
Horizontal tail:	
Airfoil	Modified NACA 63_1A012
Area, m^2 (ft^2)	2.51 (27.0)
Location of flow direction and velocity-sensor pivot point:	
Outboard from airplane centerline, m (ft)	4.41 (14.47)
Forward from leading edge of wing, m (ft)	1.06 (3.49)
Maximum control surface deflections:	
Ailerons, deg	20 up, 10 down
Stabilator, deg	15 up, 2 down
Rudder, deg	25 right, 25 left

TABLE II. MEASUREMENTS USED TO CALCULATE FLOW CORRECTIONS IN FLIGHT

Measurement	Instrument range
V_T (right and left), m/sec (mph) . . .	0 to 89.41 (0 to 200)
α (right and left), deg	−30 to 150
β (right and left), deg	−60 to 60
h, m (ft)	−152.4 to 2895.6 (−500 to 9500)
X_b-axis acceleration, a_x, g units . . .	−1 to 1
Y_b-axis acceleration, a_y, g units . . .	−1 to 1
Z_b-axis acceleration, a_z, g units . . .	−6 to 3
q, deg/sec	−100 to 100
p, deg/sec	−290 to 290
r, deg/sec	−290 to 290
$\dot{h}$, m/sec (ft/min)	−10.16 to 10.16 (−2000 to 2000)

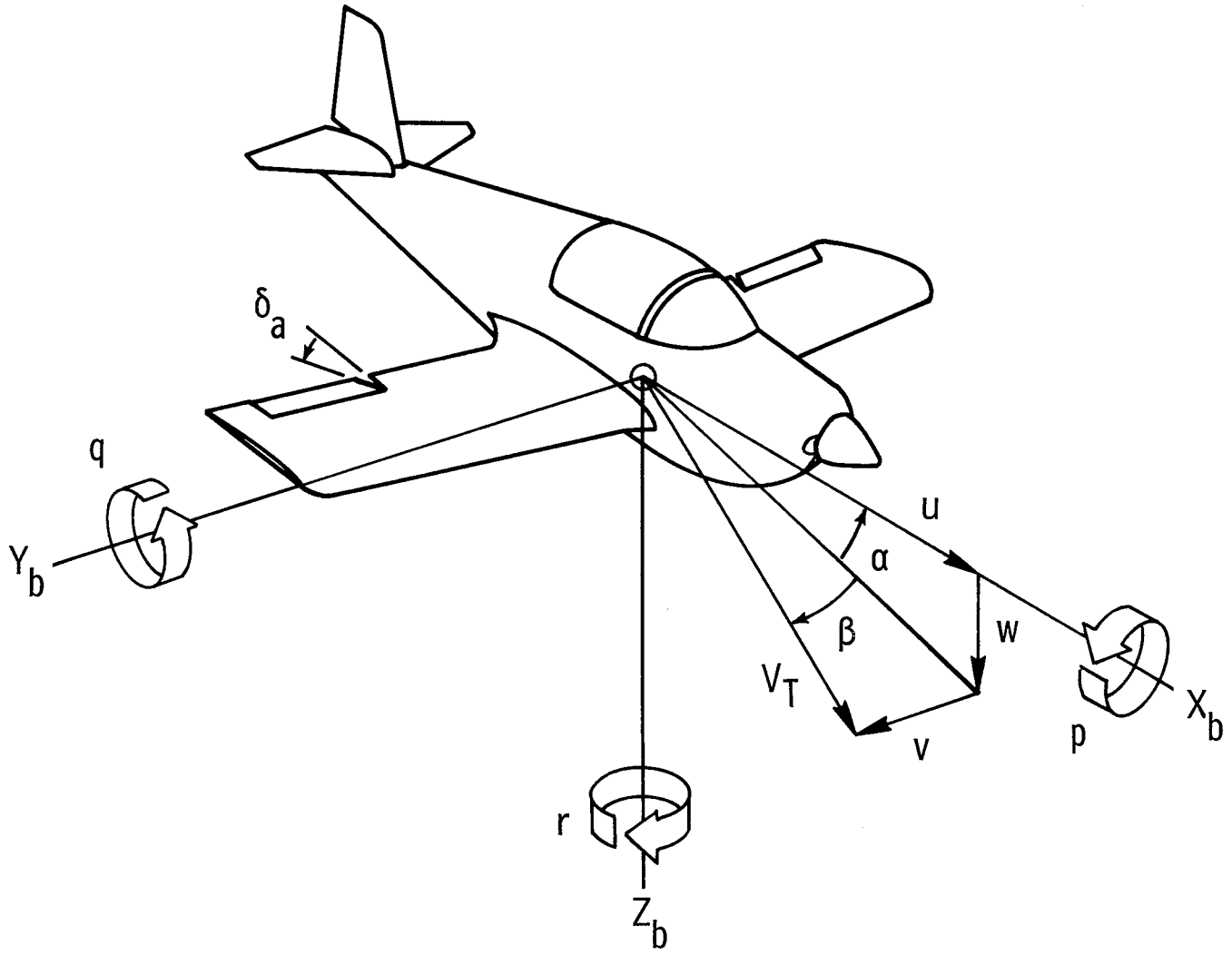

Figure 1. Definition of body axis system. Arrows indicate positive direction of quantities.

L-85-106

Figure 2. Spin research airplane in flight.

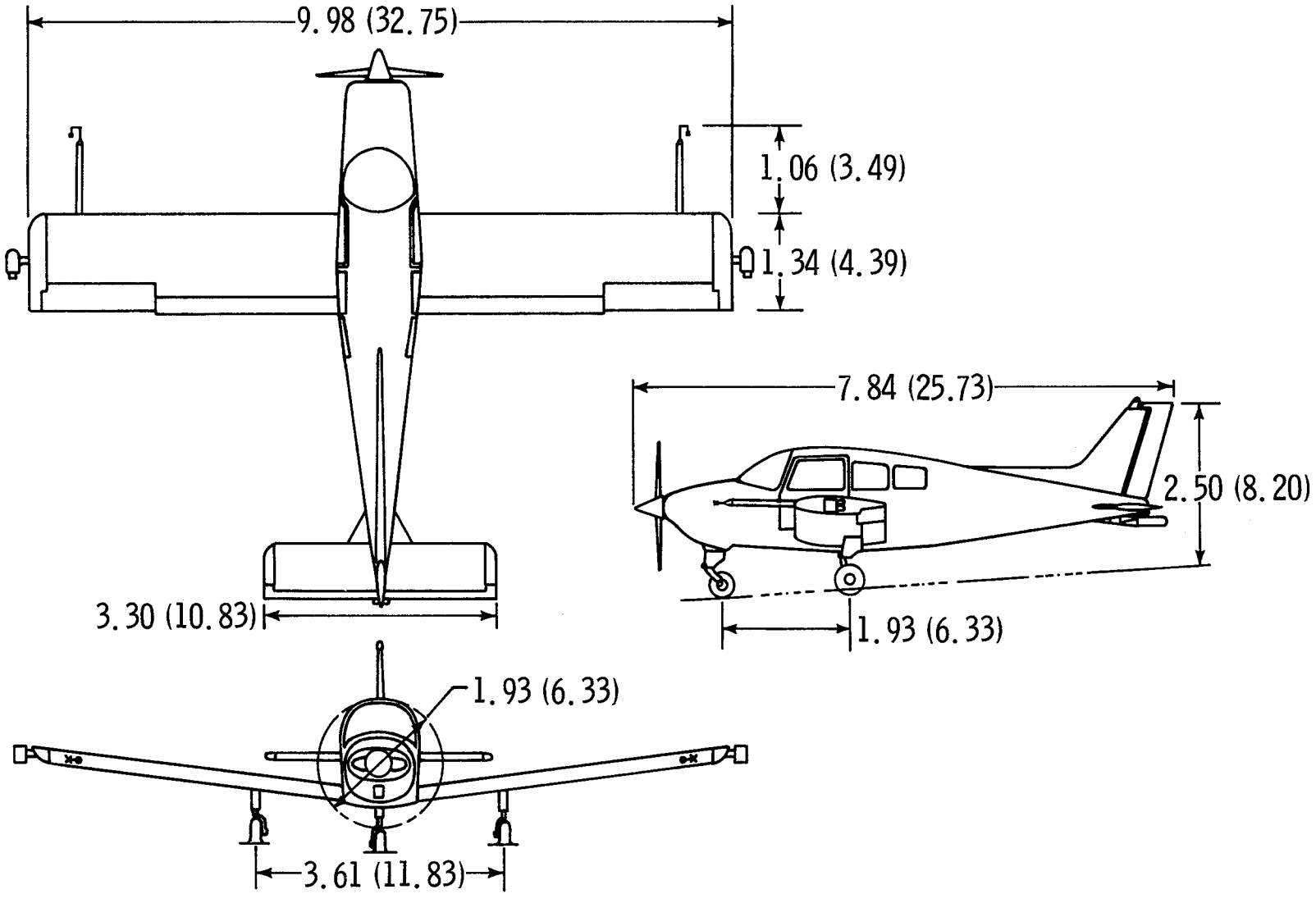

Figure 3. Three-view drawing of spin research airplane. Dimensions are given in meters (feet).

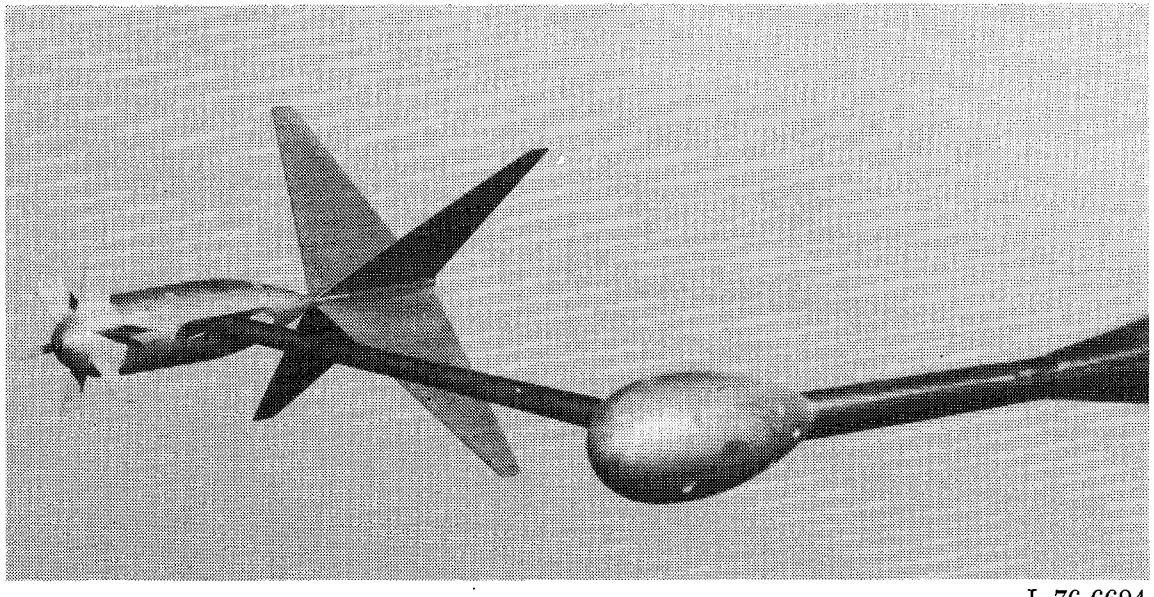

L-76-6604

Figure 4. Flow direction and velocity sensor used in flight tests.

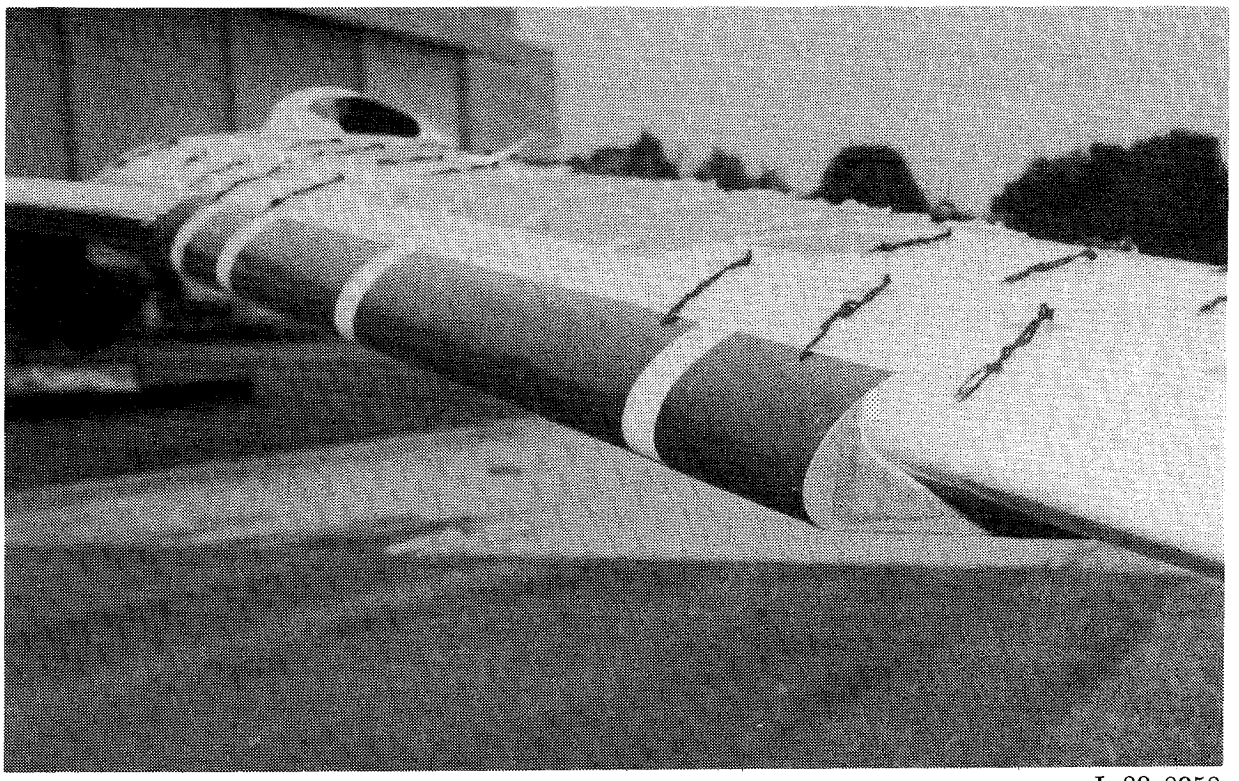

L-80-8958

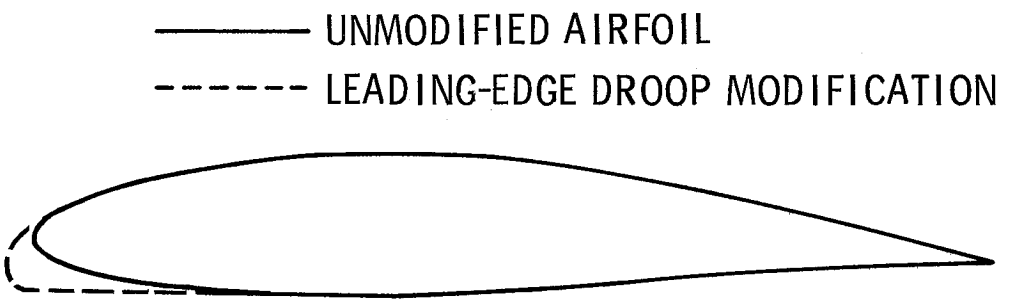

Figure 5. Photograph and sketch of wing leading-edge droop modification.

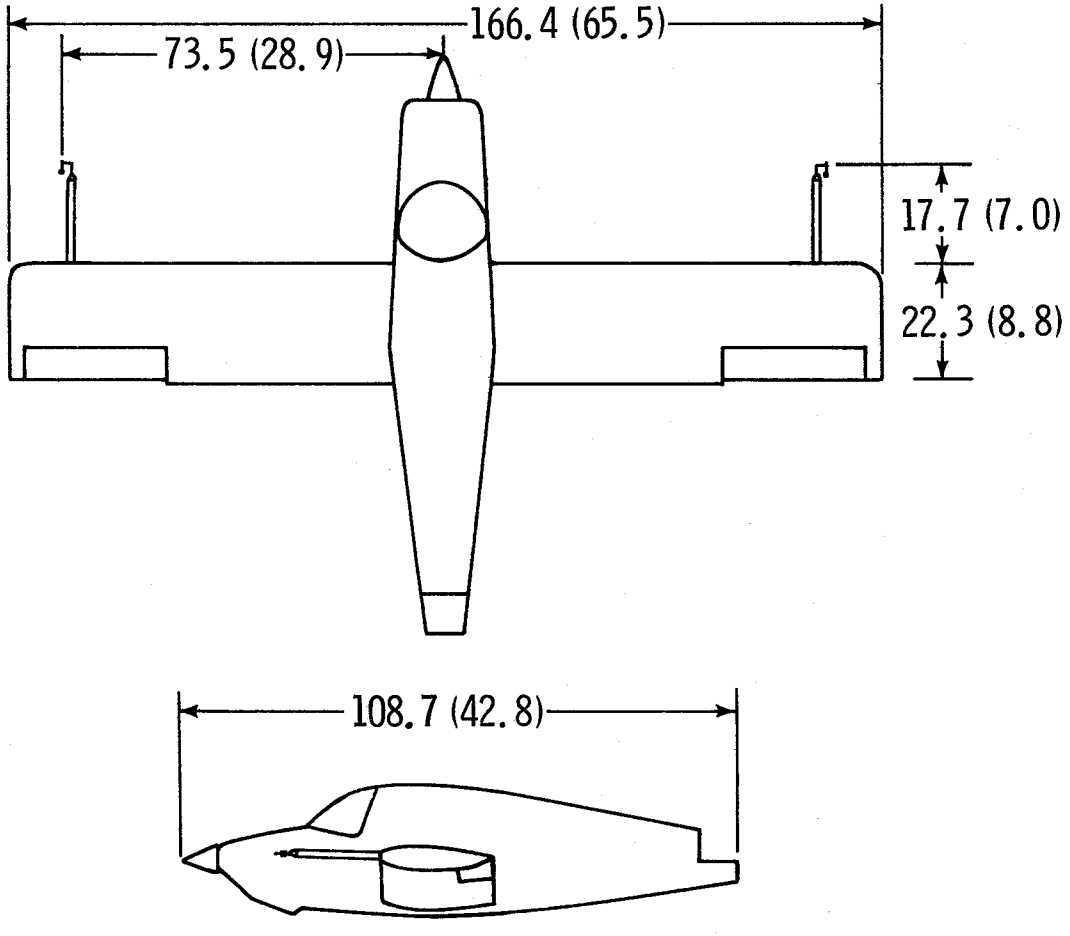

Figure 6. Drawing of 1/6-scale model. Dimensions are given in centimeters (inches).

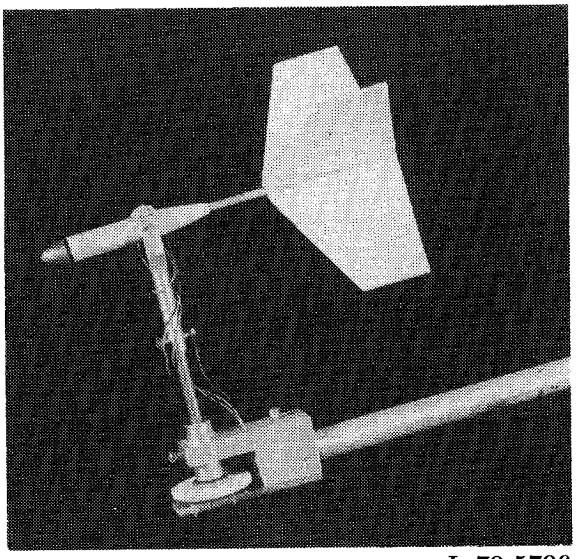

L-79-5796

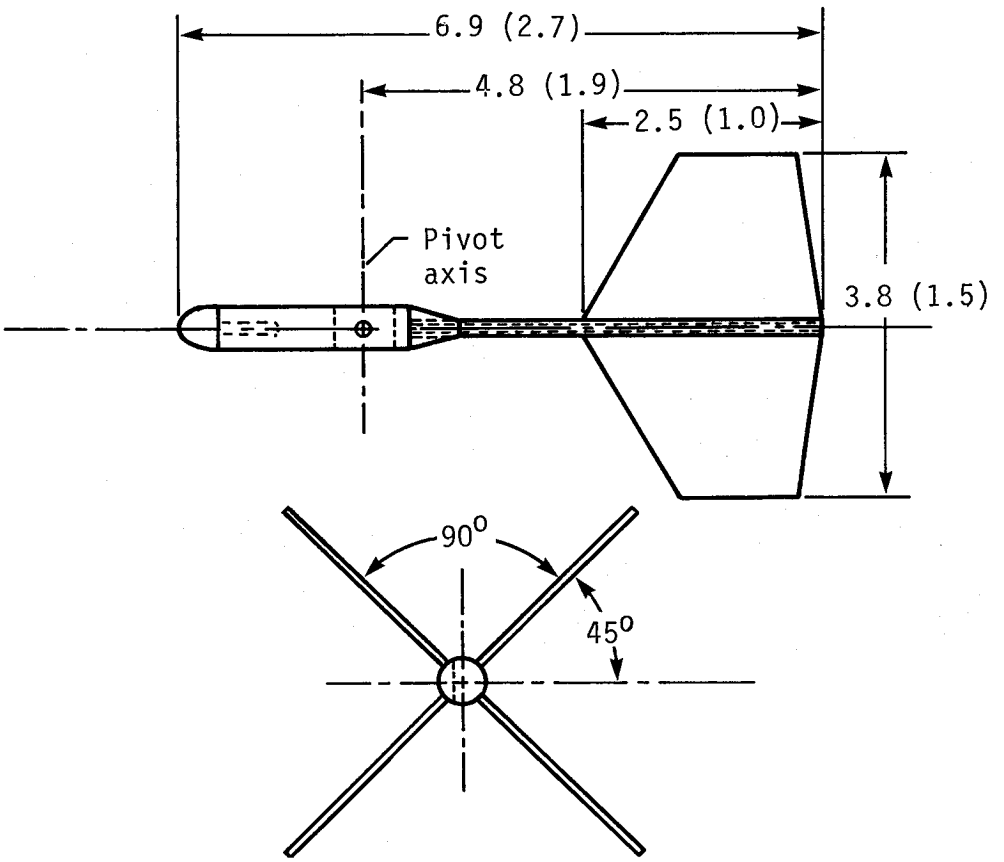

Figure 7. Photograph and sketch of flow direction sensor used in wind-tunnel tests. Dimensions are given in centimeters (inches).

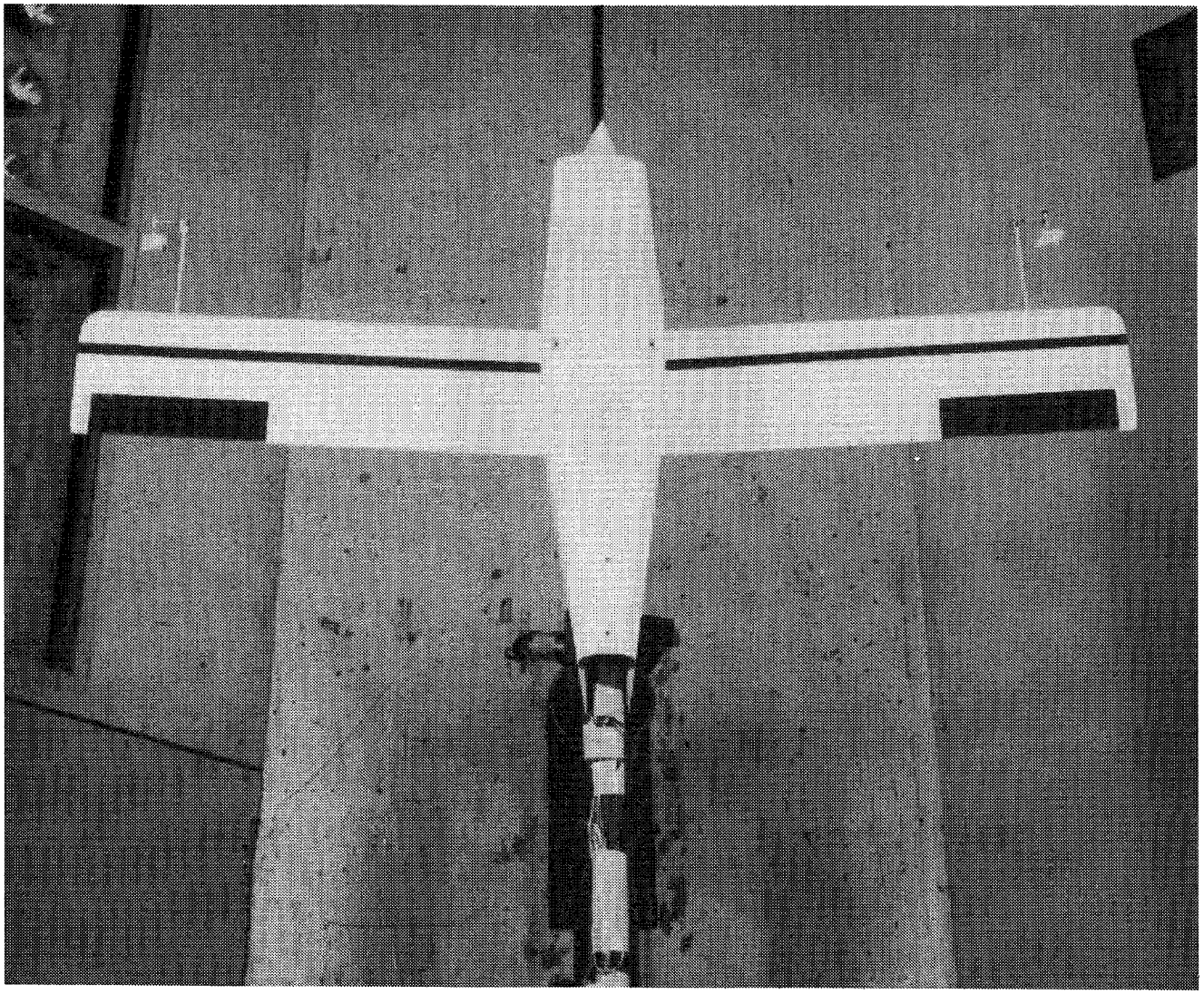

L-81-9637

Figure 8. Model mounted in the Langley 12-Foot Low-Speed Tunnel.

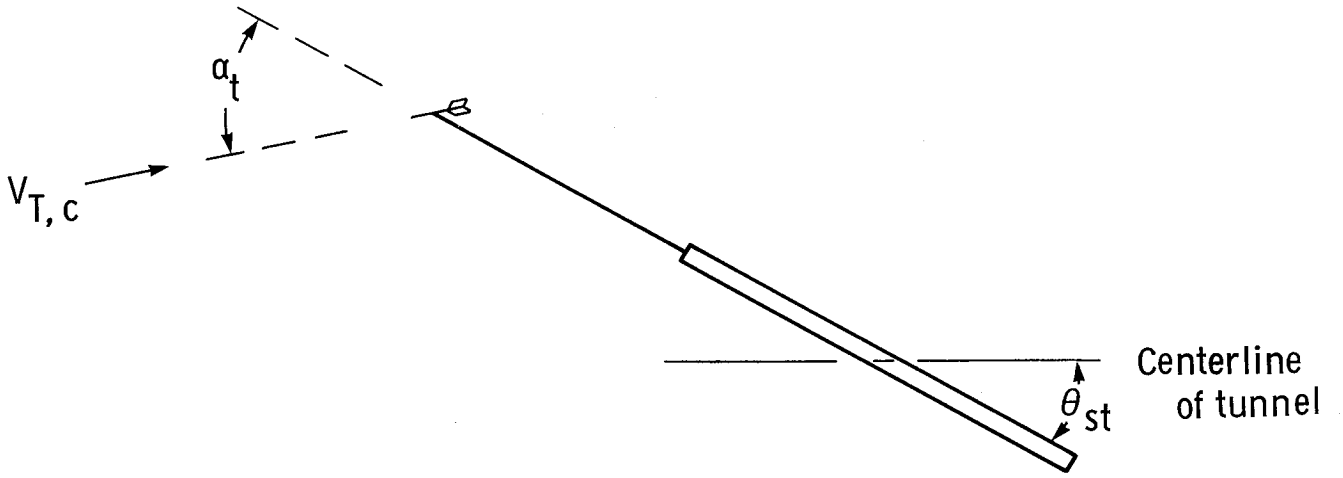

(a) Determination of true angle of attack during tunnel flow calibration.

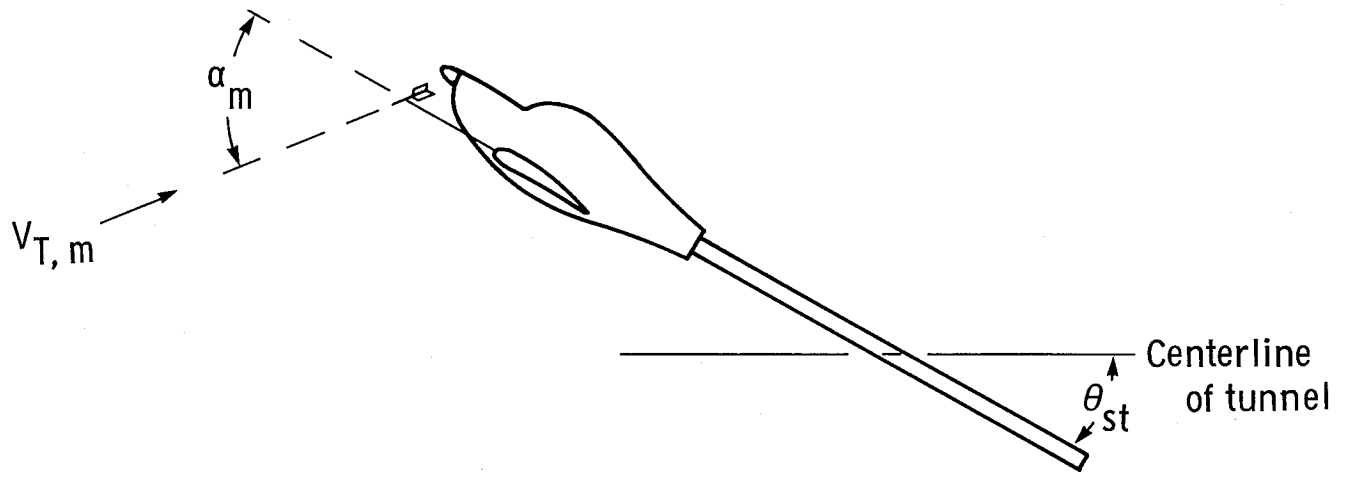

(b) Determination of measured angle of attack when sensors were mounted on model.

Figure 9. Definition of angles measured to determine the angle-of-attack flow correction.

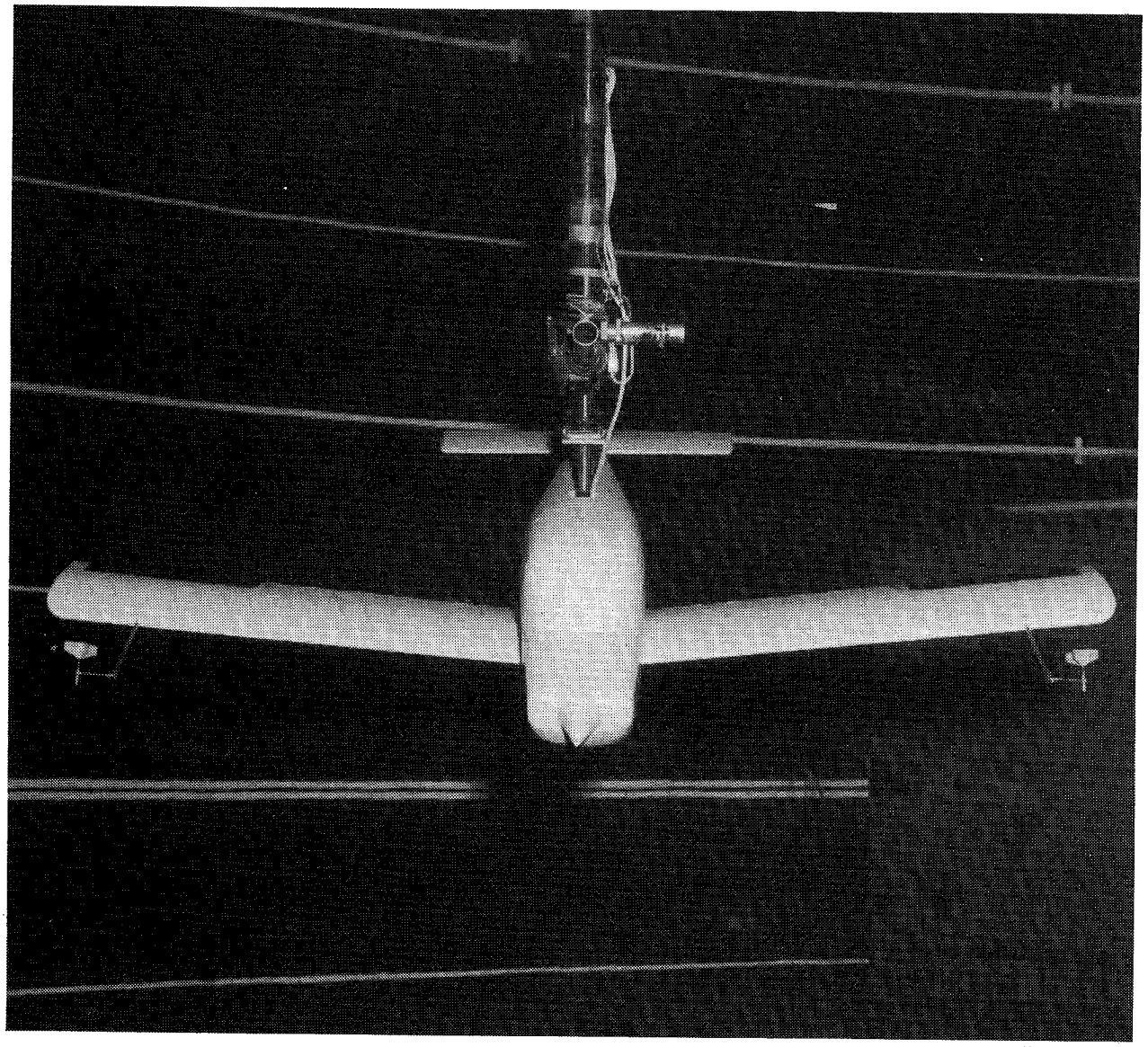

L-79-7792

Figure 10. Model mounted on rotary-balance apparatus in the Langley Spin Tunnel.

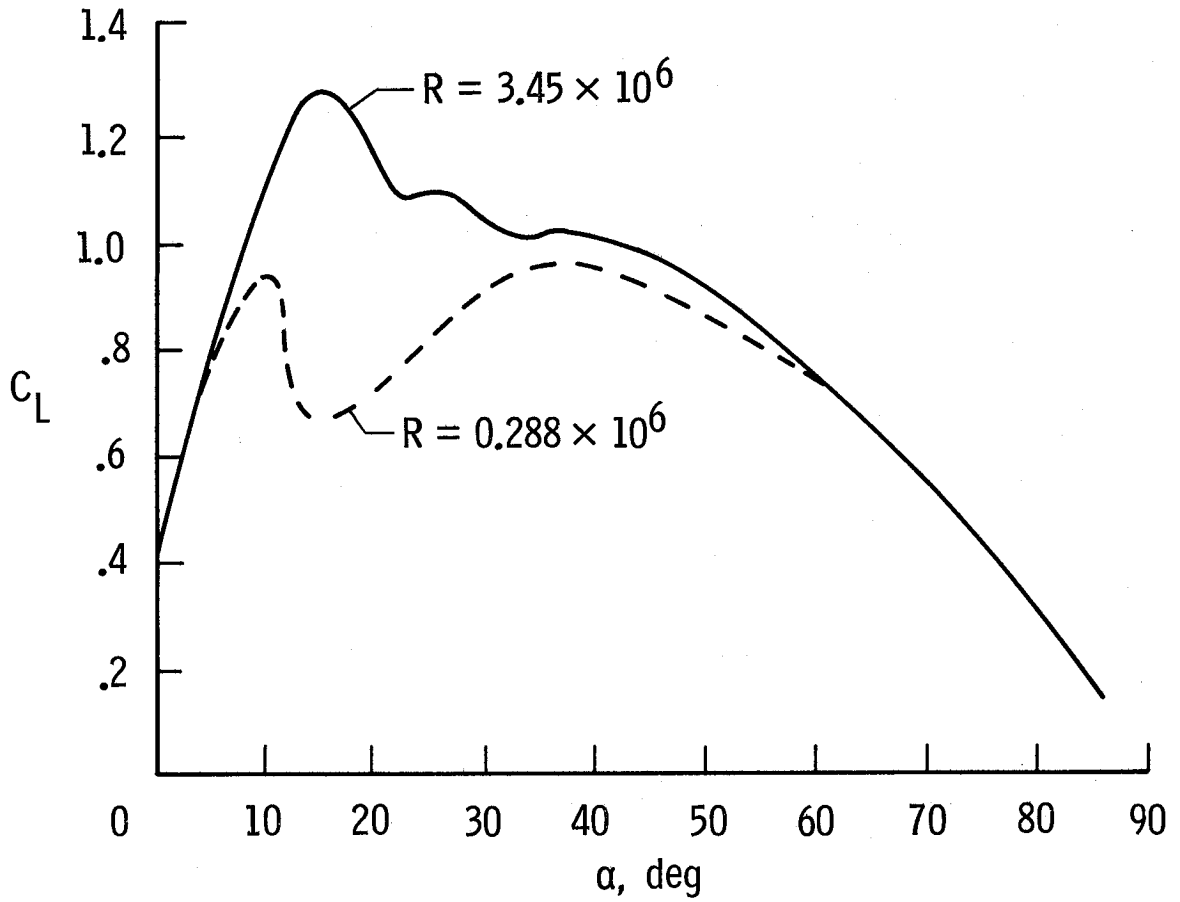

Figure 11. Effect of Reynolds number on lift characteristics of model of low-wing general aviation configuration. Data taken from reference 17.

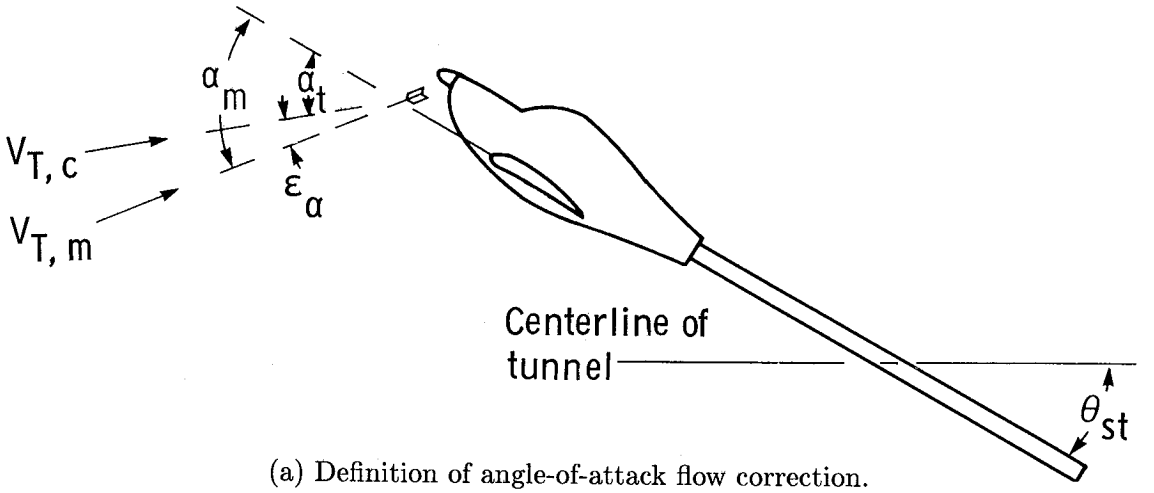

(a) Definition of angle-of-attack flow correction.

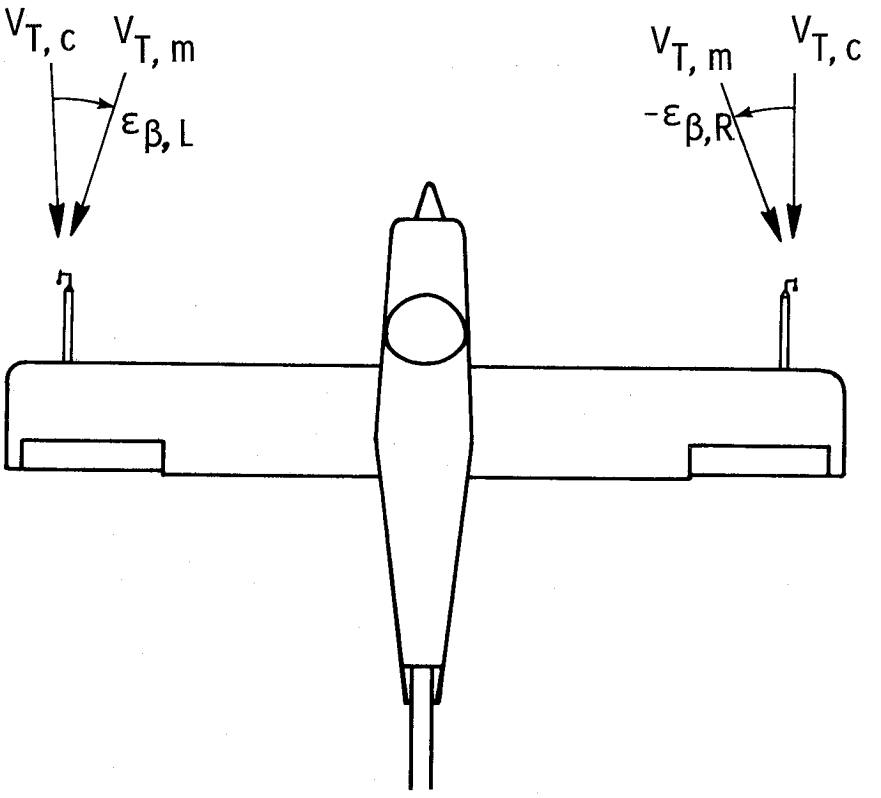

(b) Definition of angle-of-sideslip flow correction.

Figure 12. Definition of angle-of-attack and angle-of-sideslip flow corrections.

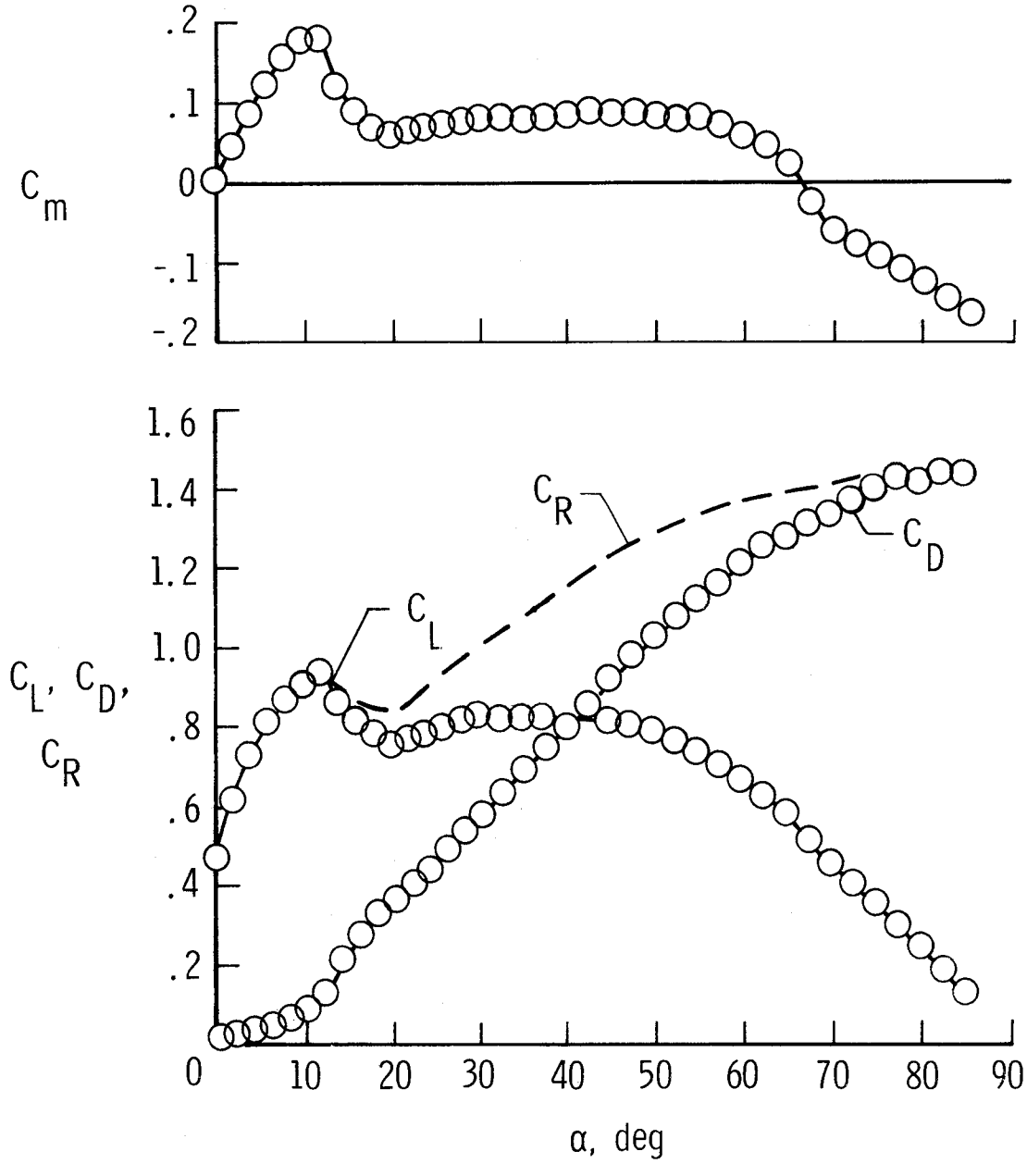

Figure 13. Longitudinal force and moment data for model with no tails. $\beta = 0°; R = 0.27 \times 10^6$.

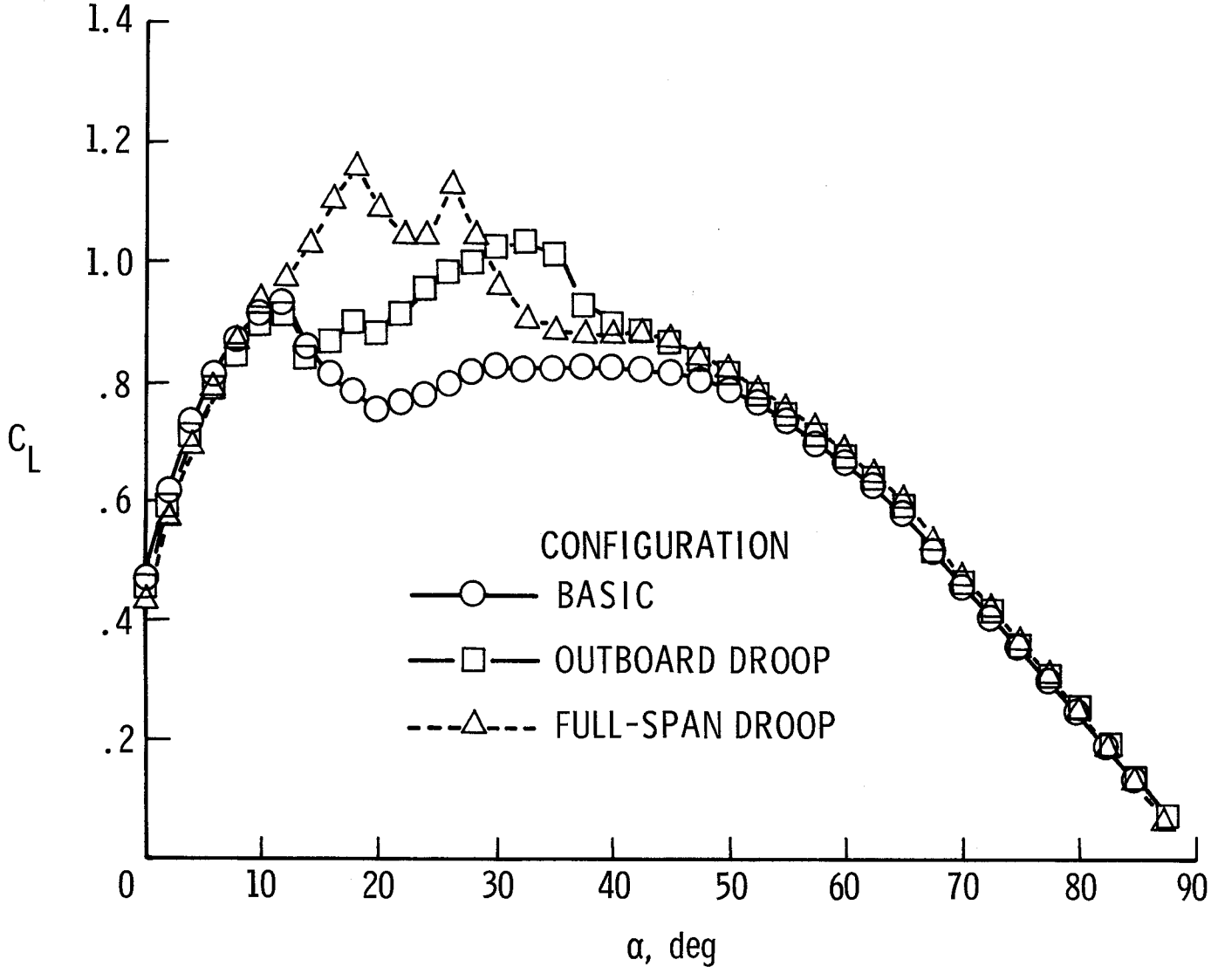

Figure 14. Effect of leading-edge modifications on lift coefficient of model with no tails. $\beta = 0°$; $R = 0.27 \times 10^6$.

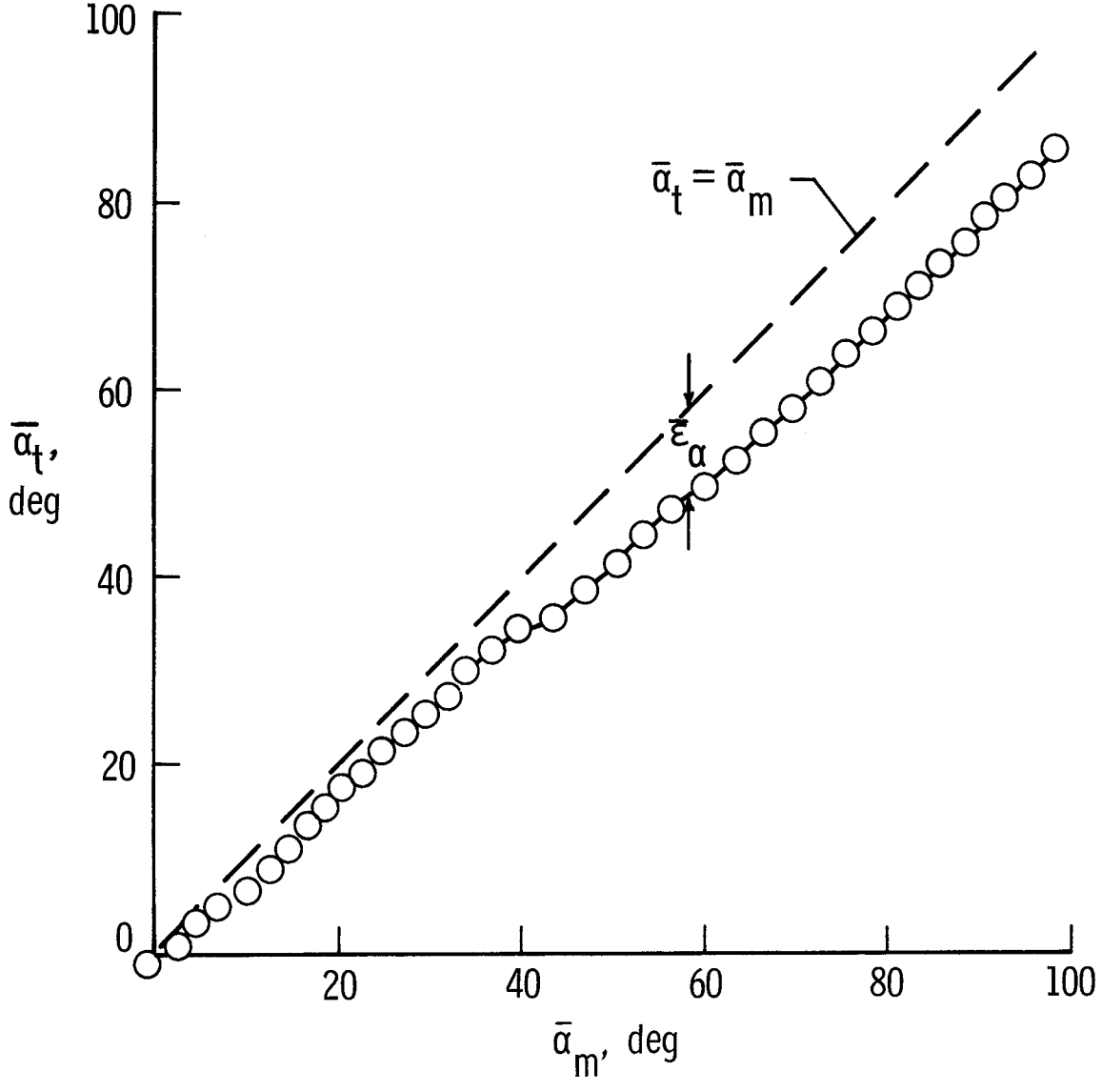

Figure 15. Average true angle of attack plotted against average measured angle of attack for basic model from static wind-tunnel tests. $\beta = 0°$; $R = 0.27 \times 10^6$.

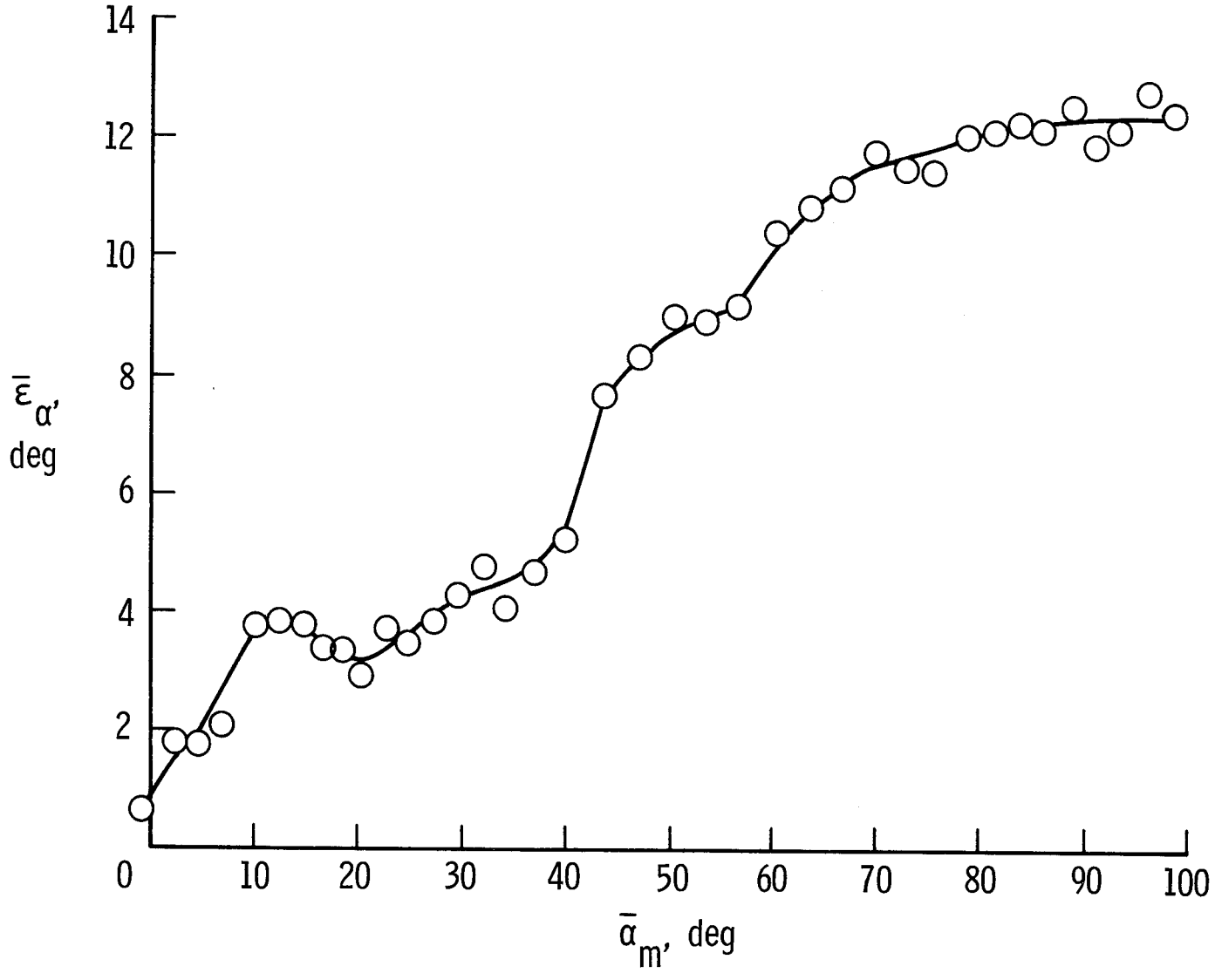

Figure 16. Average angle-of-attack flow correction for basic model determined from static wind-tunnel tests. $\beta = 0°$; $R = 0.27 \times 10^6$.

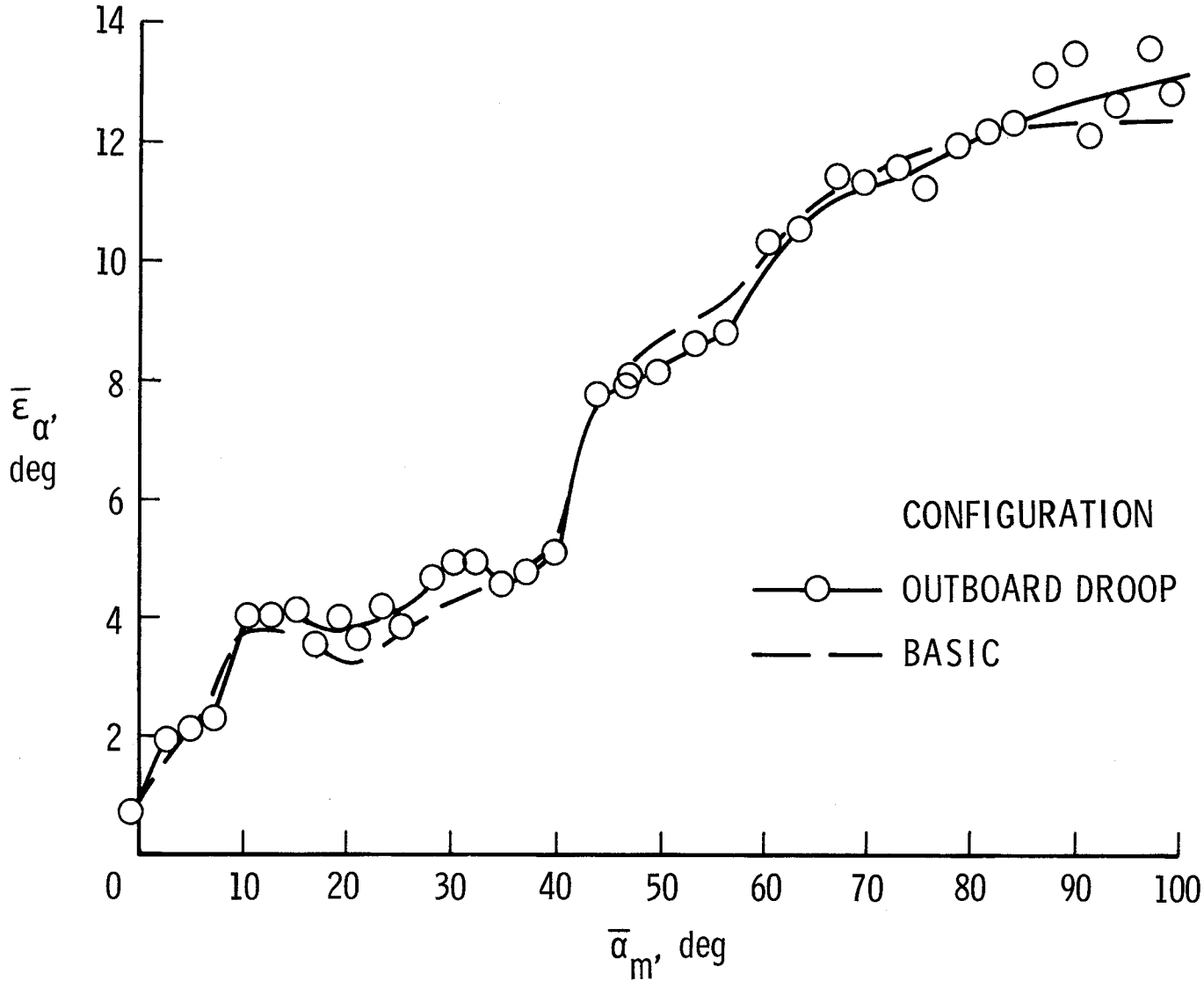

Figure 17. Effect of outboard leading-edge droop modification on average angle-of-attack flow correction determined from static wind-tunnel tests. $\beta = 0°$; $R = 0.27 \times 10^6$.

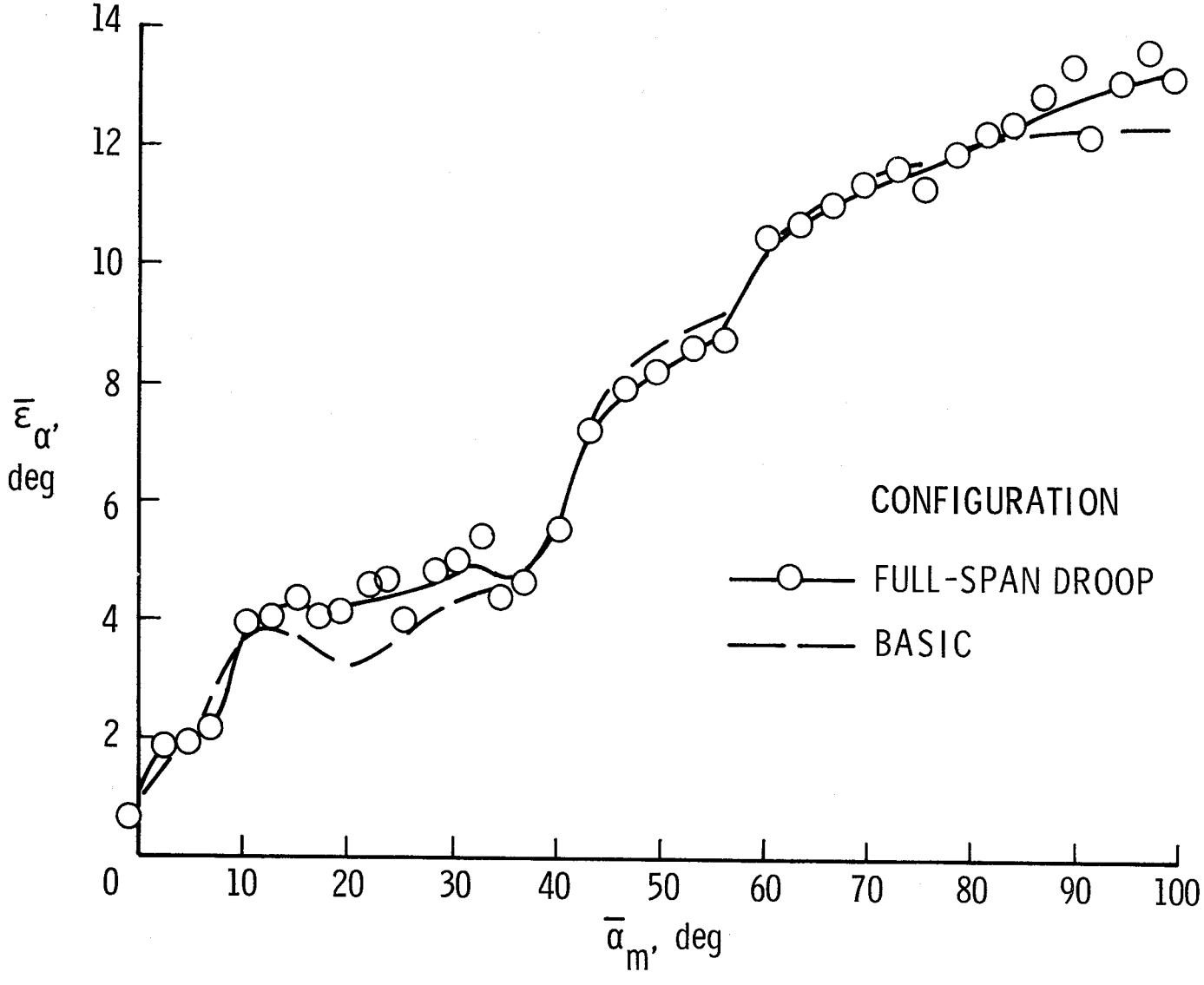

Figure 18. Effect of full-span leading-edge droop modification on average angle-of-attack flow correction determined from static wind-tunnel tests. $\beta = 0°; R = 0.27 \times 10^6$.

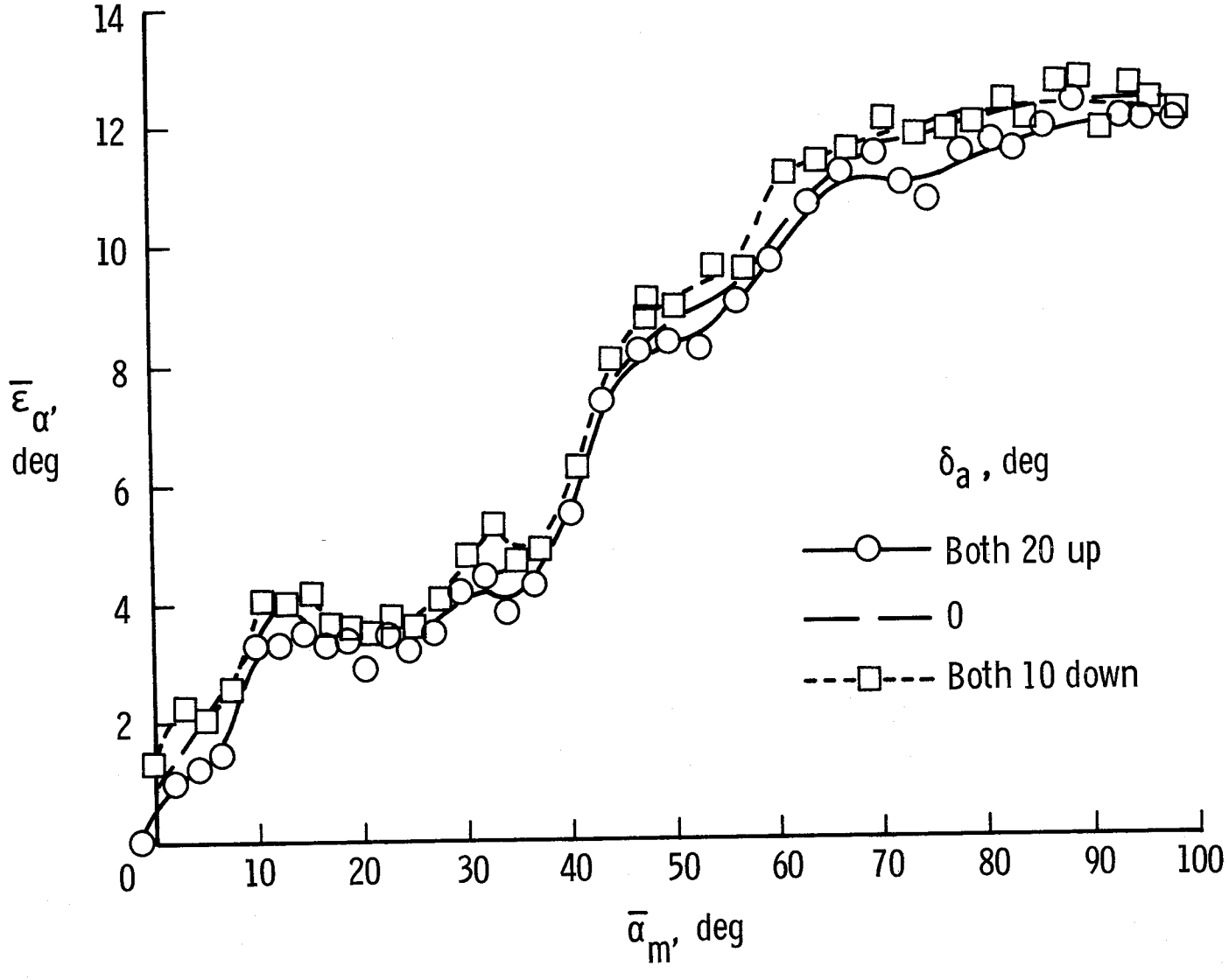

Figure 19. Effect of aileron deflections on average angle-of-attack flow correction determined from static wind-tunnel tests. $\beta = 0°$; $R = 0.27 \times 10^6$.

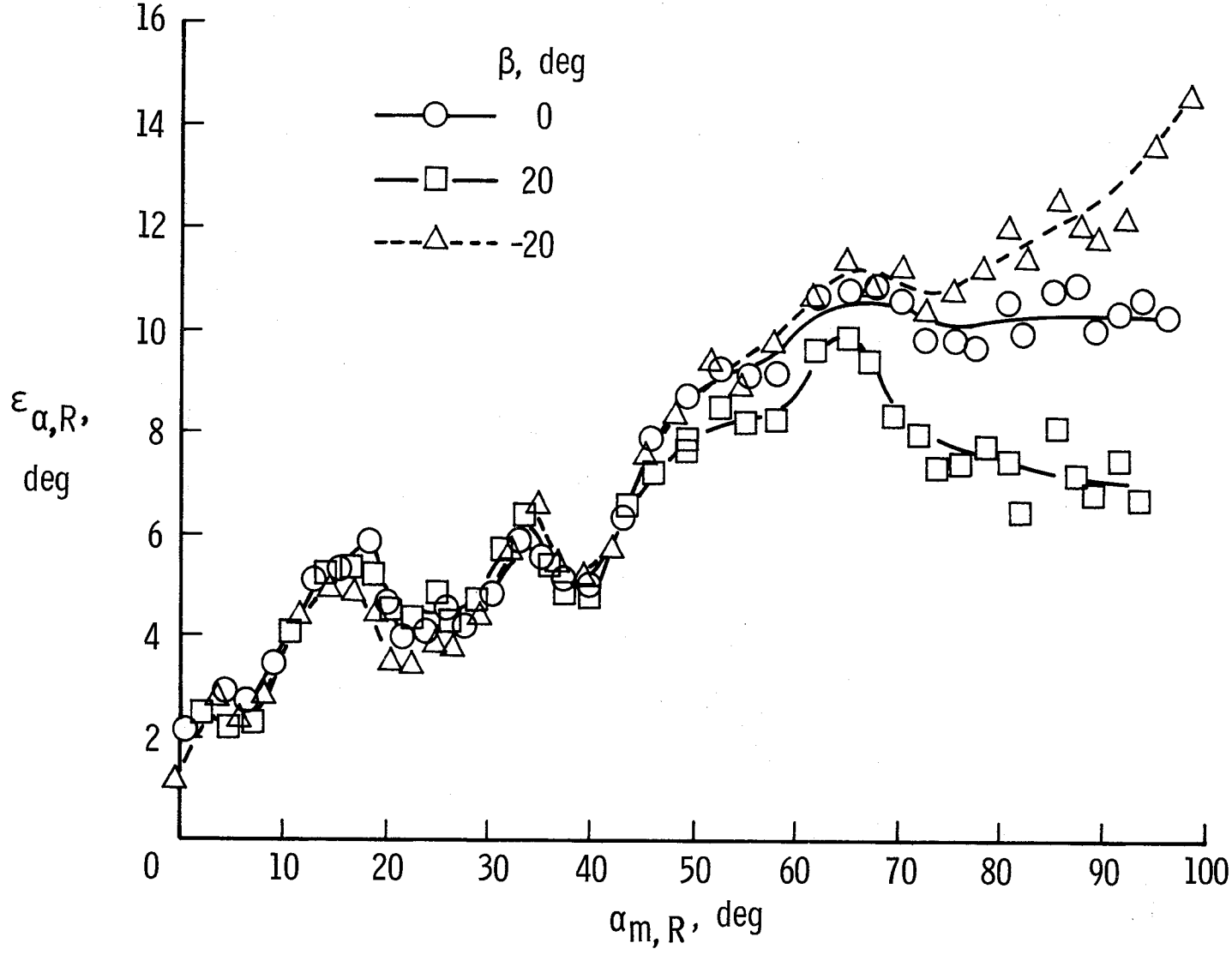

Figure 20. Effect of angle of sideslip on angle-of-attack flow correction determined from static wind-tunnel tests. $R = 0.27 \times 10^6$.

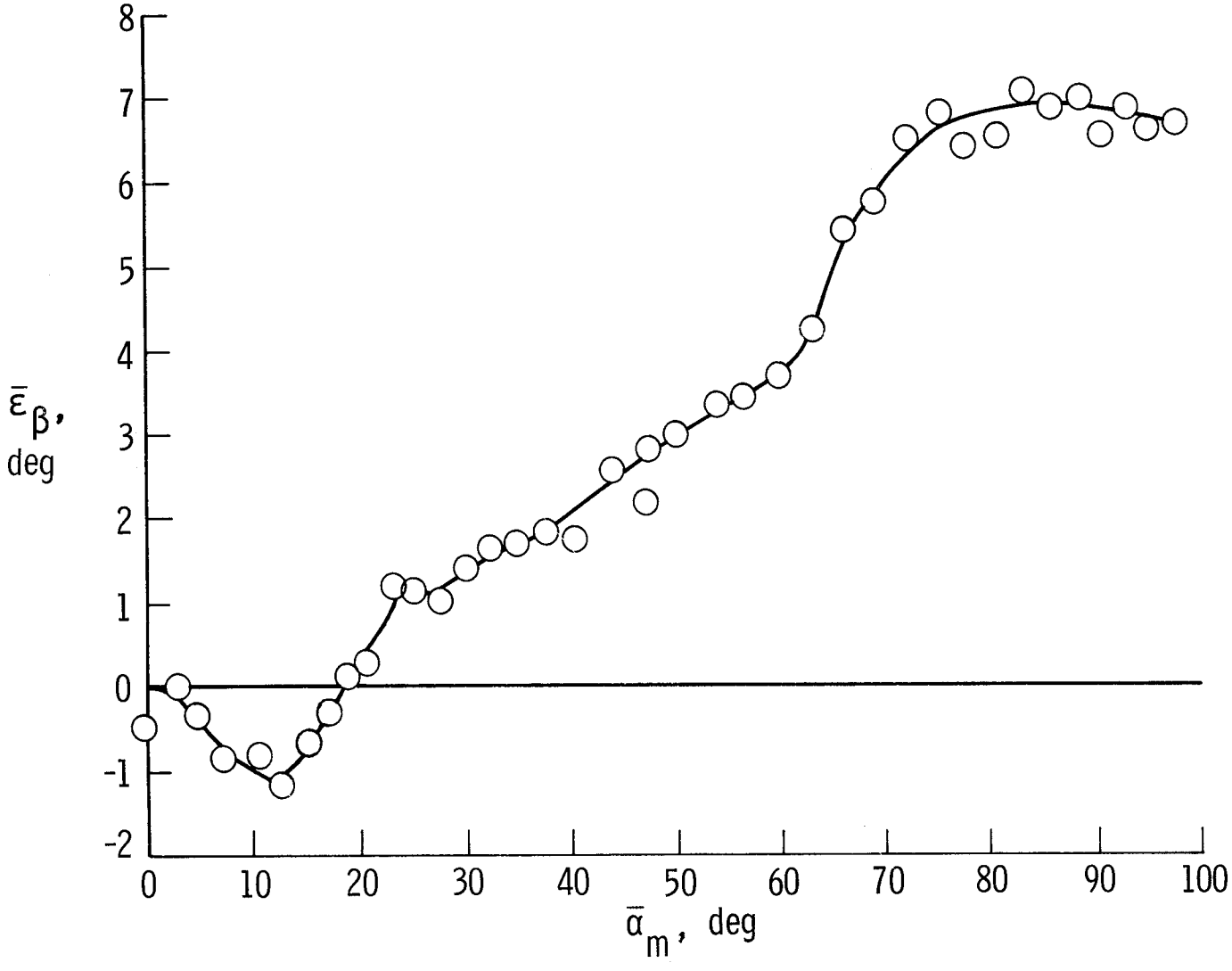

Figure 21. Average angle-of-sideslip flow correction for basic model determined from static wind-tunnel tests. $\beta = 0°; R = 0.27 \times 10^6$.

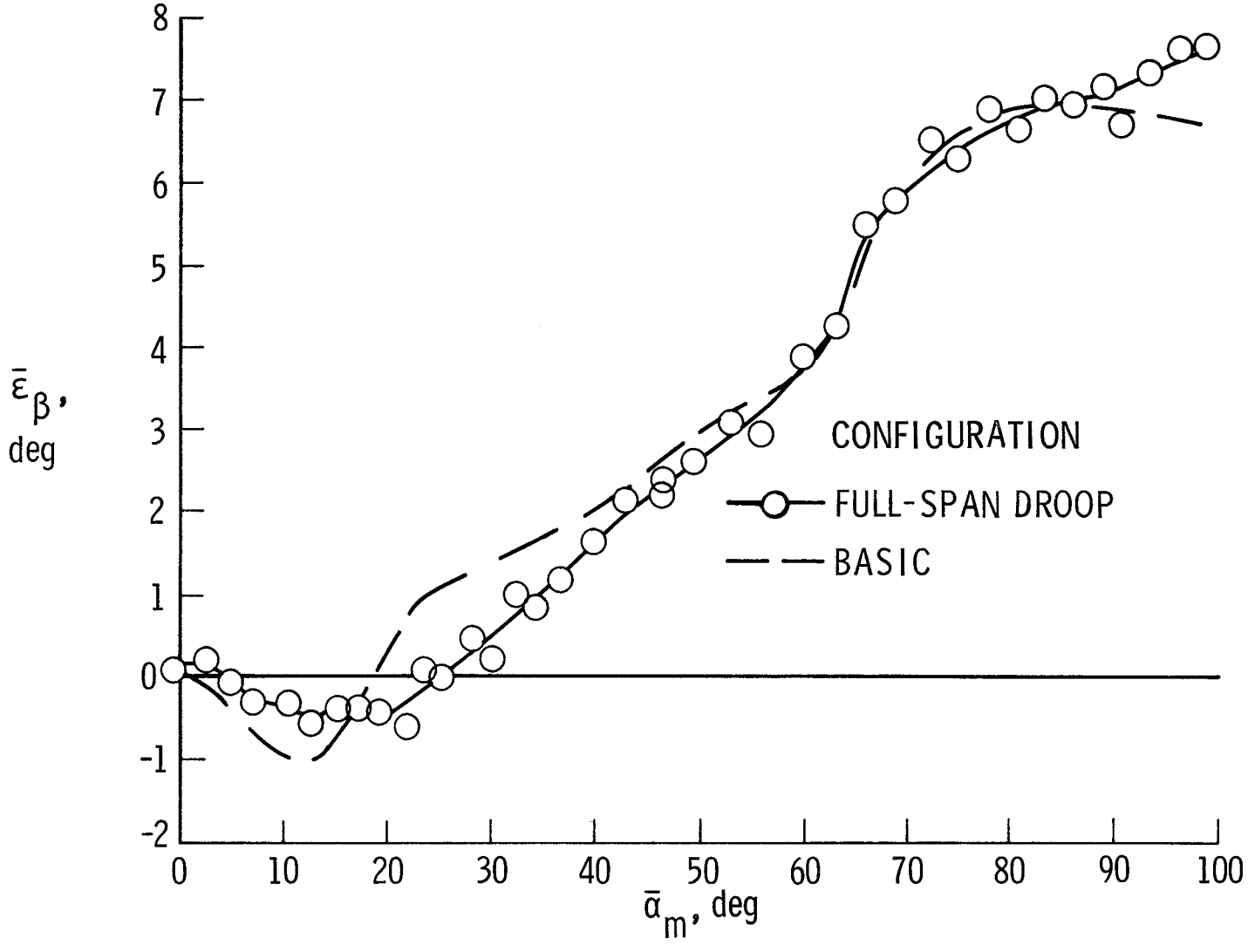

Figure 22. Effect of full-span leading-edge droop modification on average angle-of-sideslip flow correction determined from static wind-tunnel tests. $\beta = 0°$; $R = 0.27 \times 10^6$.

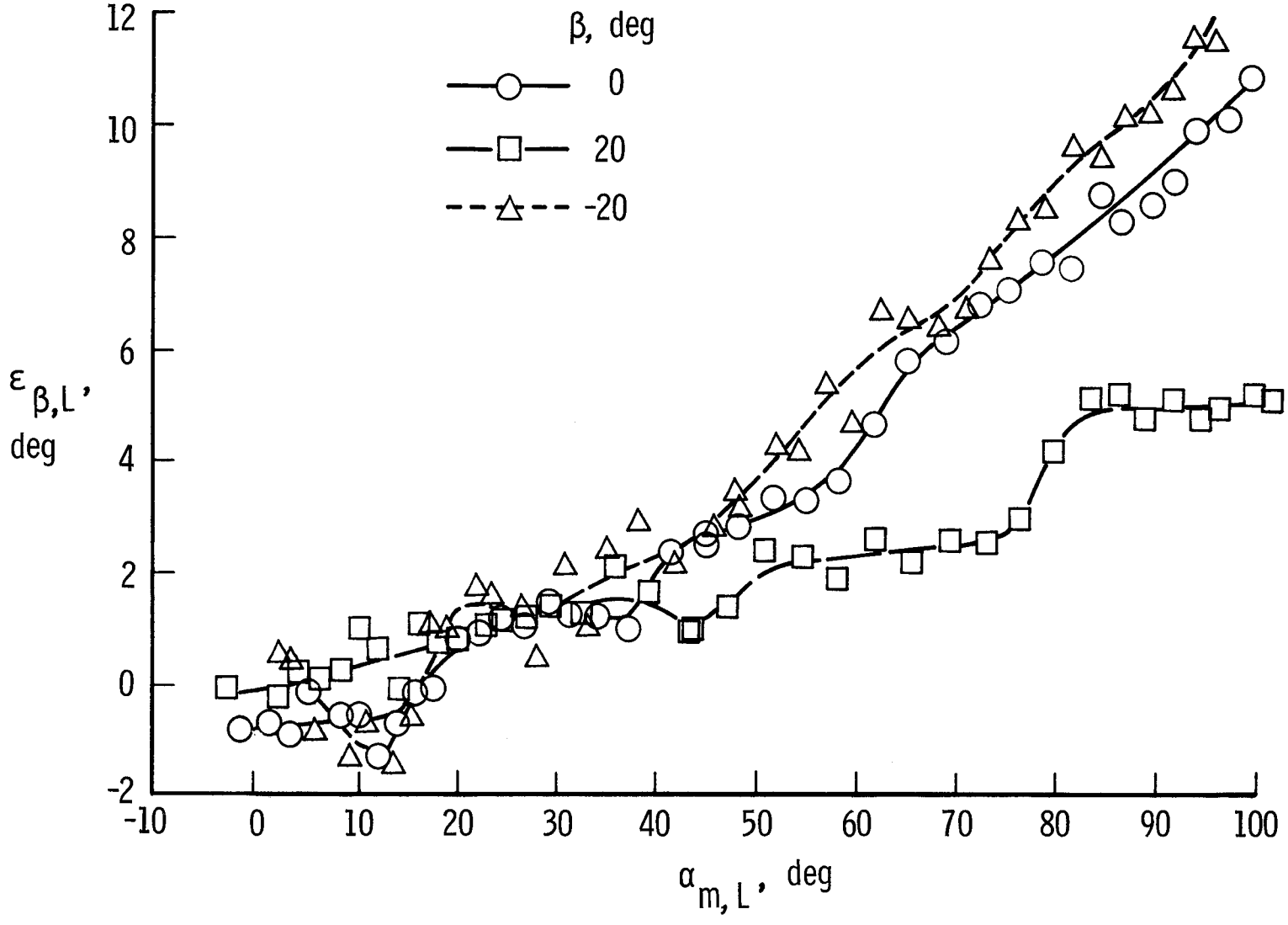

Figure 23. Effect of angle of sideslip on angle-of-sideslip flow correction determined from static wind-tunnel tests. $R = 0.27 \times 10^6$.

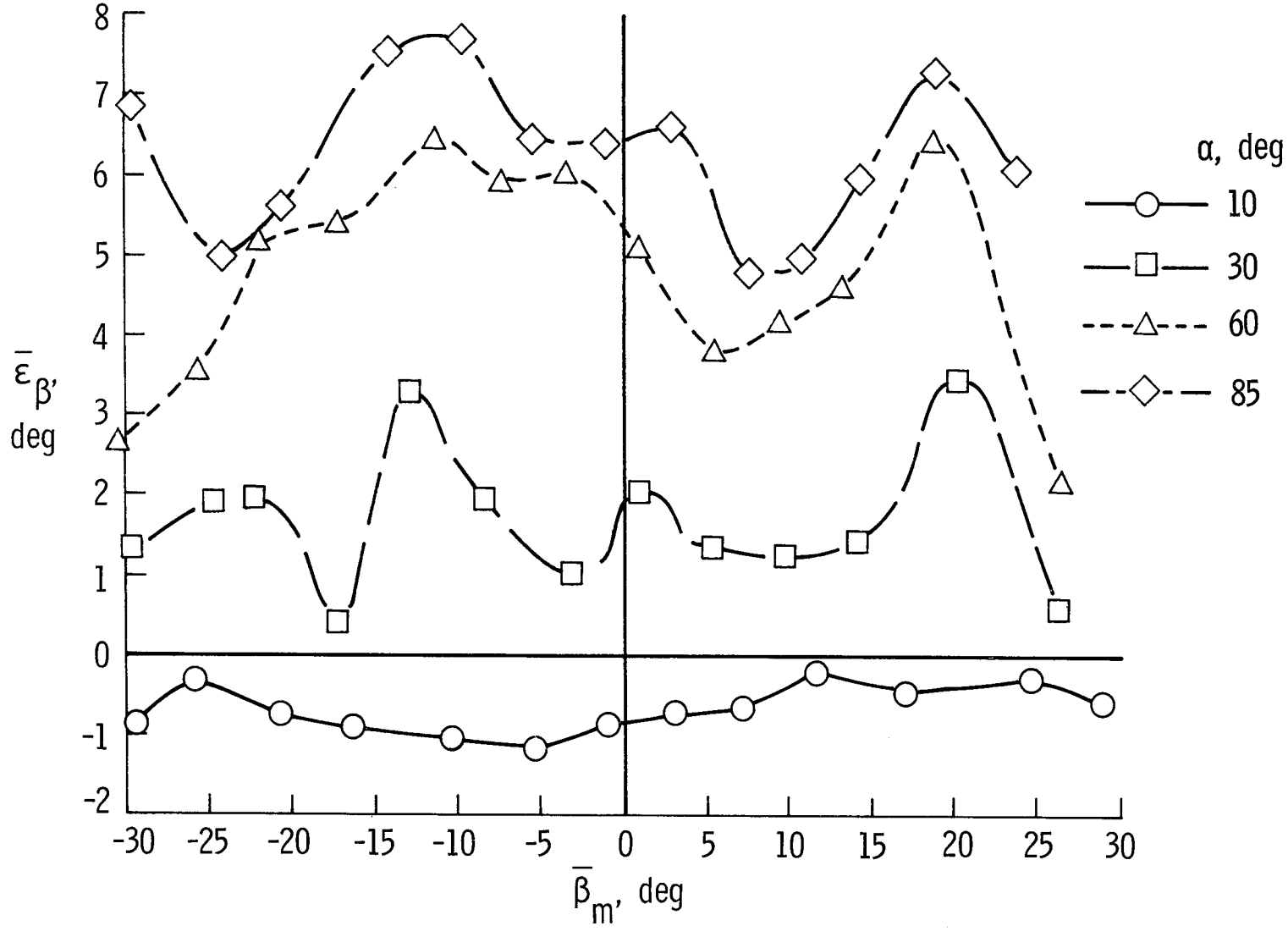

Figure 24. Effect of angle of attack on average angle-of-sideslip flow correction determined from static wind-tunnel tests. $R = 0.27 \times 10^6$.

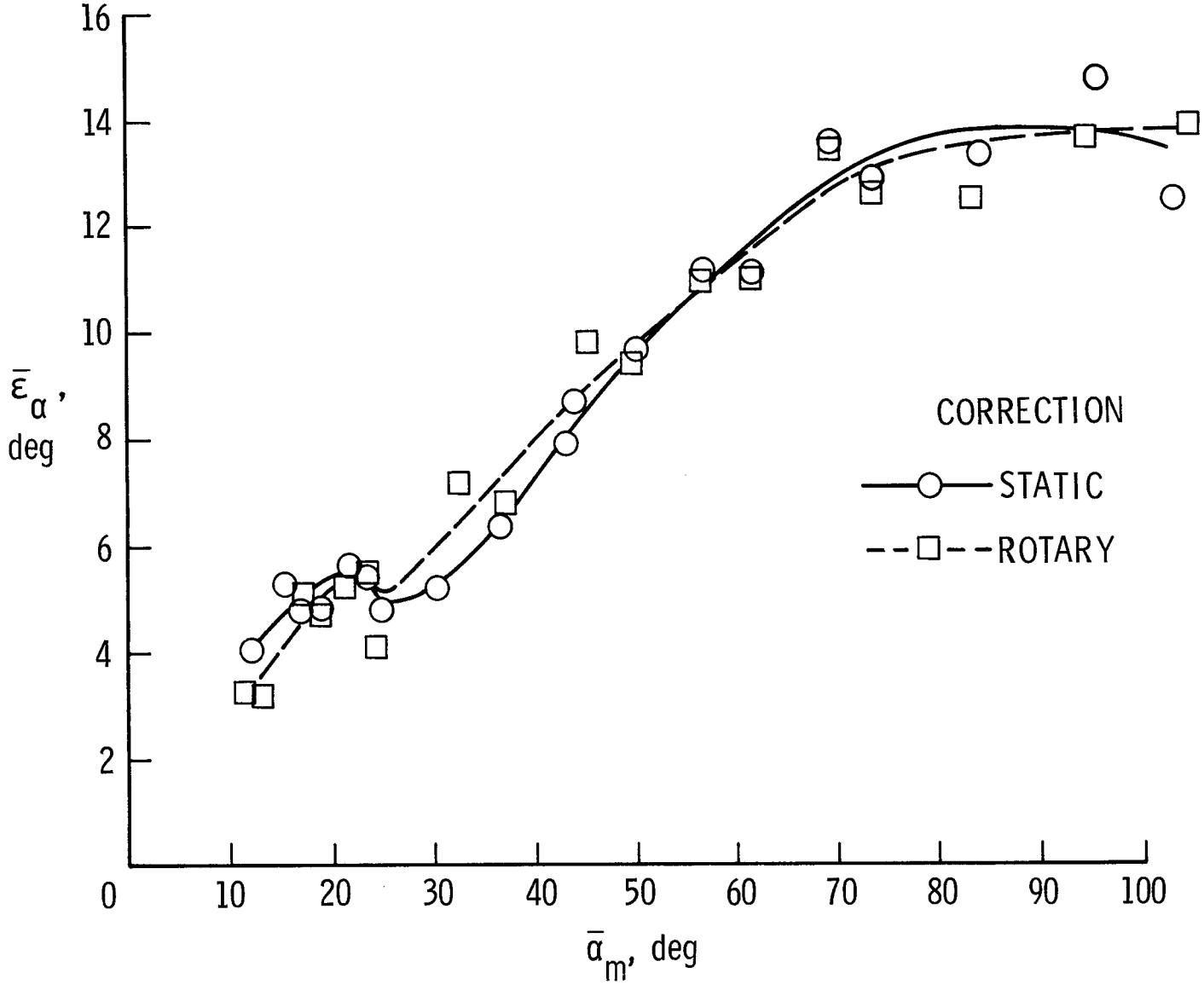

Figure 25. Effect of rotation on average angle-of-attack flow correction determined in the Langley Spin Tunnel. $R = 0.12 \times 10^6$.

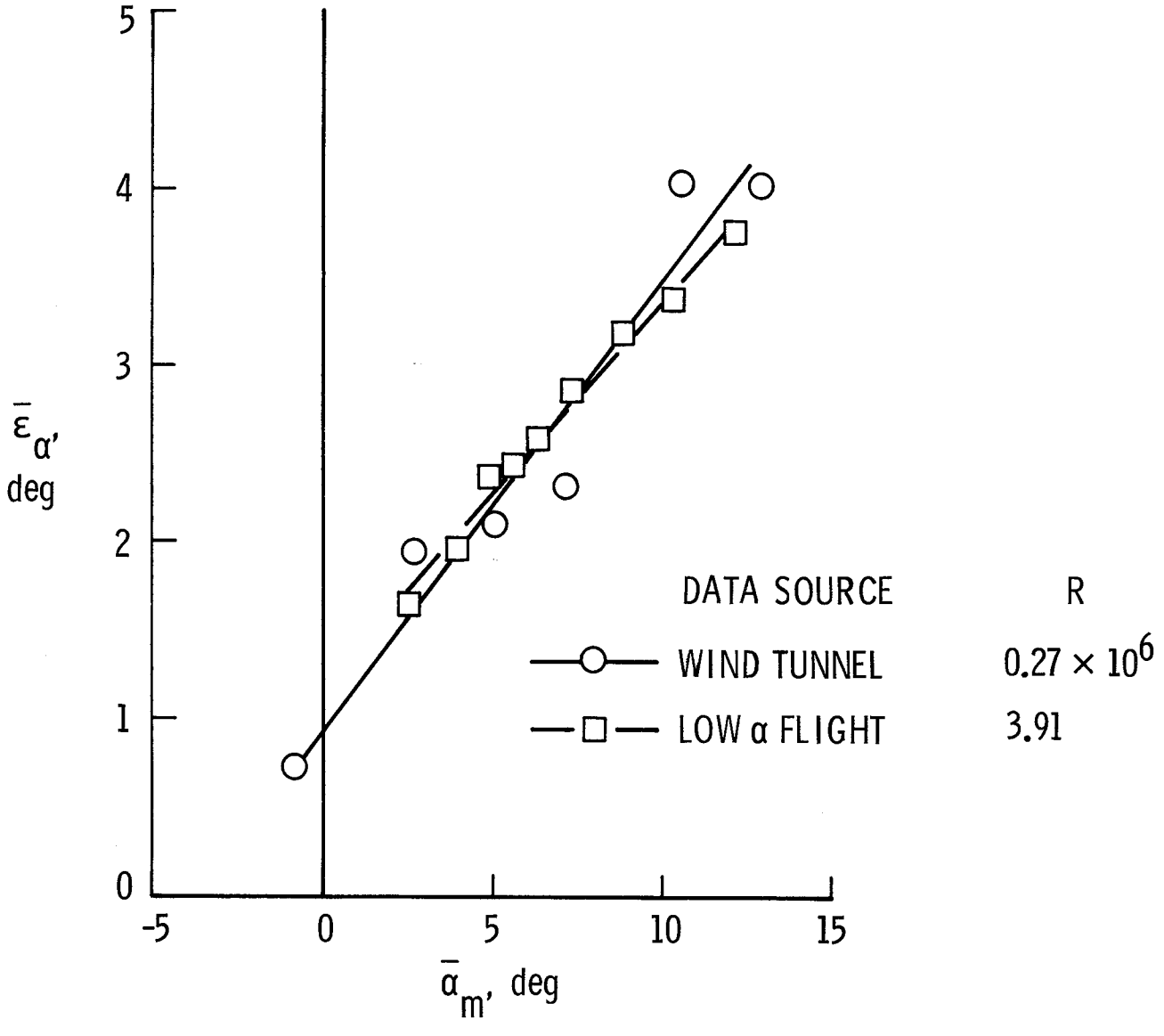

Figure 26. Comparison of average angle-of-attack flow correction determined from static wind-tunnel tests and from level flight tests of configuration with outboard leading-edge droop modification. $\beta = 0°$.

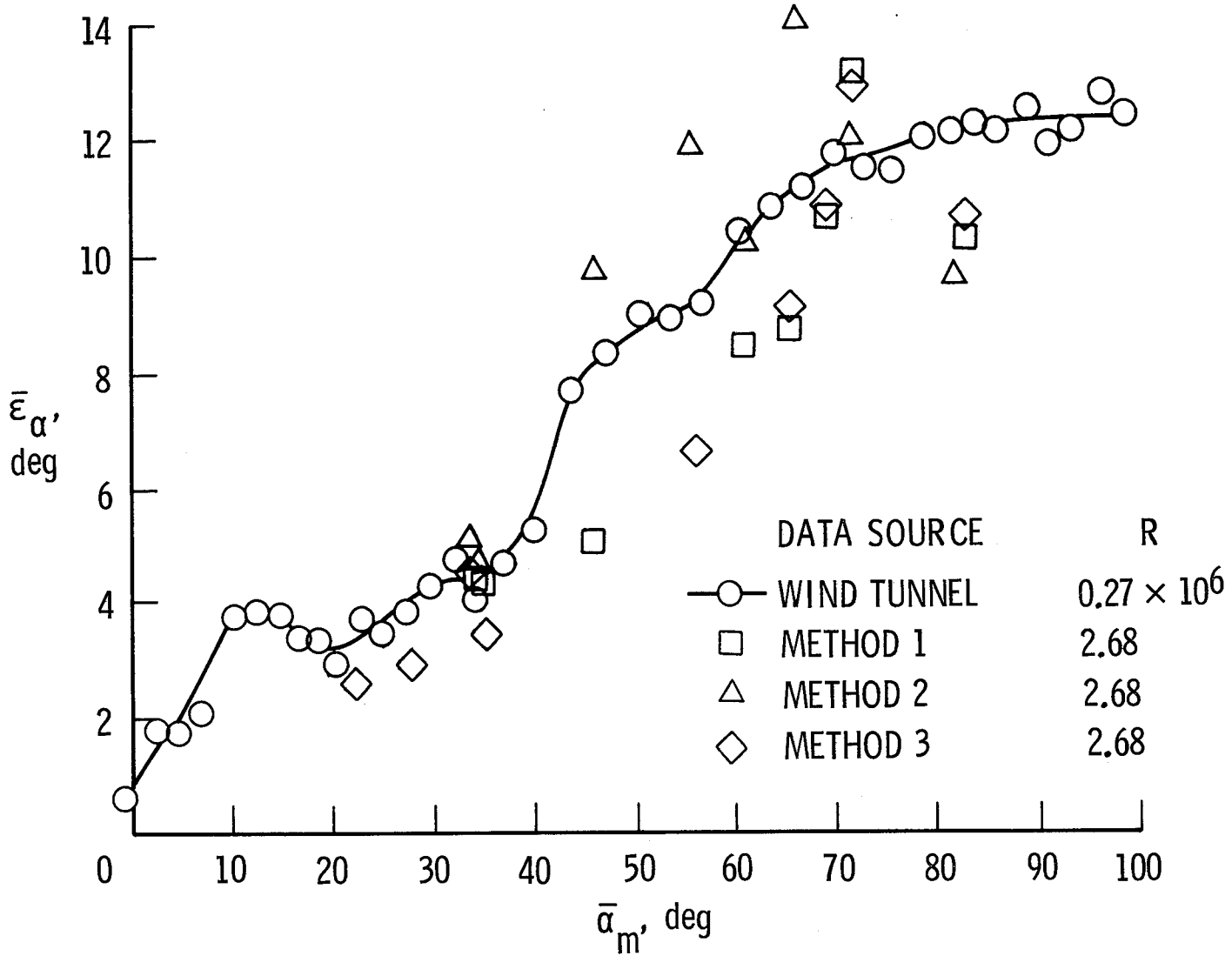

Figure 27. Comparison of results of methods 1, 2, and 3 with average angle-of-attack flow correction determined from static wind-tunnel tests.

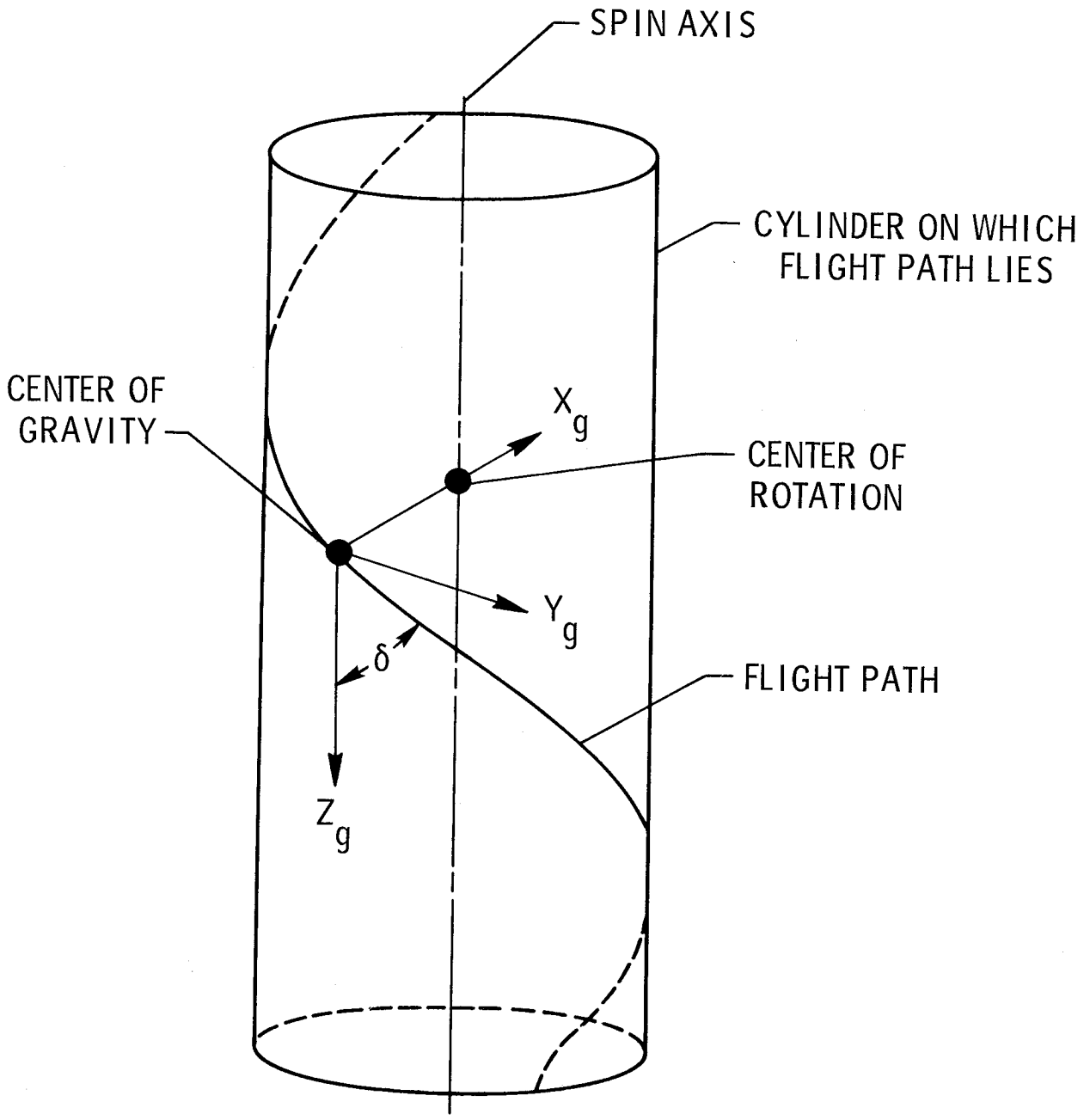

Figure 28. Instantaneous arrangement of ground axis system.

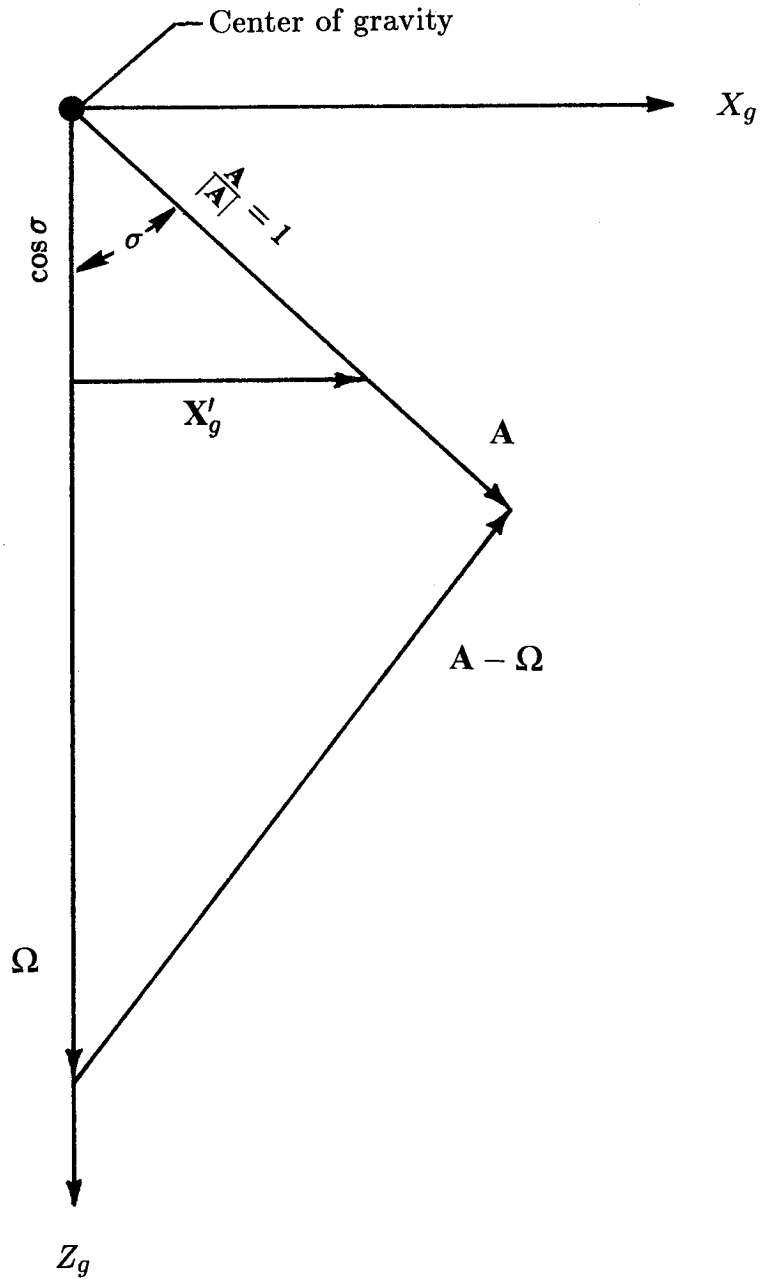

Figure 29. Relationship between resultant-acceleration and resultant-rotation vectors.

1. Report No.	2. Government Accession No.	3. Recipient's Catalog No.
NASA TM-86402		

4. Title and Subtitle	5. Report Date
Determination of Corrections to Flow Direction Sensor Measurements Over an Angle-of-Attack Range From 0° to 85°	December 1985
	6. Performing Organization Code: 505-45-43-01
7. Author(s): Thomas M. Moul	8. Performing Organization Report No.: L-15759
9. Performing Organization Name and Address: NASA Langley Research Center, Hampton, VA 23665-5225	10. Work Unit No.
	11. Contract or Grant No.
12. Sponsoring Agency Name and Address: National Aeronautics and Space Administration, Washington, DC 20546-0001	13. Type of Report and Period Covered: Technical Memorandum
	14. Sponsoring Agency Code

15. Supplementary Notes

This paper is a shortened version of a thesis submitted in partial fulfillment of the requirements for the Degree of Master of Science, George Washington University, Washington, D.C., August 1983.

16. Abstract

An investigation has been conducted into the nature of corrections for angle-of-attack and angle-of-sideslip measurements obtained with sensors mounted in front of each wingtip of a general aviation airplane. These flow corrections have been obtained from both wind-tunnel and flight tests over an angle-of-attack range from 0° to 85°. Both the angle-of-attack and angle-of-sideslip flow corrections were found to be substantial. The corrections were a function of the angle of attack and angle of sideslip and were fairly insensitive to configuration changes and rotational effects. The angle-of-attack flow correction determined from the static wind-tunnel tests agreed reasonably well with the correction determined from flight tests.

17. Key Words (Suggested by Authors(s))	18. Distribution Statement
Angle-of-attack measurement Flow direction sensor calibration Upwash Spin flight testing	Unclassified—Unlimited Subject Category 05

19. Security Classif.(of this report)	20. Security Classif.(of this page)	21. No. of Pages	22. Price
Unclassified	Unclassified	50	A03

For sale by the National Technical Information Service, Springfield, Virginia 22161

NASA-Langley, 1985